

Robust Image Retrieval-based Visual Localization using Kapture

Martin Humenberger, Yohann Cabon, Nicolas Guerin, Julien Morat, Vincent Leroy, Jérôme Revaud, Philippe Rerole, Noé Pion, Cesar de Souza, and Gabriela Csurka

NAVER LABS Europe, France
<https://europe.naverlabs.com>
 firstname.lastname@naverlabs.com

Abstract

Visual localization tackles the challenge of estimating the camera pose from images by using correspondence analysis between query images and a map. This task is computation and data intensive which poses challenges on thorough evaluation of methods on various datasets. However, in order to further advance in the field, we claim that robust visual localization algorithms should be evaluated on multiple datasets covering a broad domain variety. To facilitate this, we introduce *kapture*, a new, flexible, unified data format and toolbox for visual localization and structure-from-motion (SfM). It enables easy usage of different datasets as well as efficient and reusable data processing. To demonstrate this, we present a versatile pipeline for visual localization that facilitates the use of different local and global features, 3D data (e.g. depth maps), non-vision sensor data (e.g. IMU, GPS, WiFi), and various processing algorithms. Using multiple configurations of the pipeline, we show the great versatility of *kapture* in our experiments. Furthermore, we evaluate our methods on eight public datasets where they rank top on all and first on many of them. To foster future research, we release code, models, and all datasets used in this paper in the *kapture* format open source under a permissive BSD license.

github.com/naver/kapture

github.com/naver/kapture-localization

1. Introduction

Visual localization is an important component of many location-based systems such as self-driving cars [45, 127], autonomous robots [63], or augmented, mixed, and virtual reality [12, 69, 67]. The goal is to estimate the accurate position and orientation of a camera from captured images. In more detail, correspondences between a representation

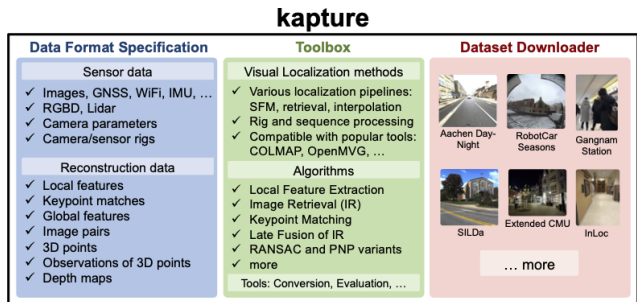


Figure 1. Kapture consists of a detailed sensor and reconstruction data specification, I/O and conversion tools, visual localization methods, and a dataset downloader that directly provides datasets in the kapture format.

of the environment (map) and a query image are utilized to estimate the camera pose in 6 degrees of freedom (DOF). Environmental changes caused by time of day or season of the year, but also structural changes on house facades or store fronts, large view point changes between mapping and query images, as well as people, cars, or other dynamic objects that occlude parts of the scene, pose critical challenges on visual localization methods.

Methods. Visual localization is an active research field and many approaches have been proposed. Structure-based methods [89, 70, 90, 64, 102, 95] use local features to establish correspondences between 2D query images and 3D reconstructions. These correspondences are then used to compute the camera pose using perspective-n-point (PNP) solvers [54] within a RANSAC loop [38, 26, 60, 17]. To reduce the search range in large 3D reconstructions, image retrieval methods [75, 84] can be used to first retrieve most relevant images from the SfM model. Second, local correspondences are established in the area defined by those images.

Scene point regression methods [99, 19, 20, 62, 21] establish the 2D-3D correspondences using a deep neural network (DNN) and absolute pose regression meth-

ods [52, 59, 16, 94, 51, 22] directly estimate the camera pose with a DNN. Another strategy is to estimate the pose of an image by directly aligning deep image features with a reference 3D model [85].

Image retrieval can also be used for visual localization when no 3D map is available. The camera pose of a query image can be computed from the poses of top retrieved database images by interpolating retrieved image poses [107, 119, 108, 94], estimating the relative pose between query and retrieved images [126, 121], estimating absolute pose from 2D-2D matches [124], via relative pose regression [16, 34] or by building local 3D models on the fly [108, 75].

Furthermore, objects [114, 82, 27, 11] or semantic information [37] can also be used for visual localization.

Processing. For many visual localization algorithms, large neural networks have to be trained and executed, and large-scale SFM reconstructions have to be computed. Considering the fact that even medium sized datasets for visual localization often consist of more than 1000 images, this typically makes it a computationally intensive task. Furthermore, since the structure of the map is often domain, application, and method specific, it needs to be separately constructed for each dataset and sometimes even for each experiment. Given the algorithmic challenges mentioned above, we claim that visual localization or SFM algorithms should be evaluated on multiple datasets covering broad in-domain and/or cross-domain variety. Even if these datasets exist (see Section 4.1), evaluation comes with the burden that datasets are often provided in different formats including different coordinate systems and camera parameter representations.

To facilitate data processing for visual localization, SFM, sensor fusion, and related fields such as visual simultaneous localization and mapping (VSLAM), in this paper we first introduce a new toolbox called *kapture* (see Figure 1). We then use it to implement a versatile processing pipeline which we evaluate on eight popular datasets with various parameter settings and pipeline configurations.

Our pipeline is inspired by structure-based methods that use image retrieval to select the image pairs used for local feature matching. This approach has the following advantages that strengthen our choice: (i) it allows convenient integration of data-driven methods, most notably for image retrieval and local feature matching, (ii) while still providing the benefits of accurate pose computation using a geometric pipeline. Finally, (iii) as will be shown in Section 4.7, such methods are applicable on a variety of datasets and applications scenarios.

Image features. As a consequence, most relevant to our work are data-driven local [73, 33, 36, 79, 29, 66, 113] and global [8, 77, 78] image features. Using those, recent advances in the field showed great results on tasks like image

matching [76, 104] and visual localization [84, 36, 80, 39, 75]. Motivated by the good performance reported for the local feature R2D2 [79] on visual localization and the global feature APGeM [78] on landmark retrieval, in this paper, using *kapture* and our proposed pipeline, we further evaluate the performance of such methods on multiple visual localization datasets.

Contributions. Summarizing, this paper makes the following contributions: **First**, we propose a toolbox called *kapture* that consists of a unified data format as well as processing tools for visual localization and structure from motion. **Second**, using *kapture*, we propose a versatile localization pipeline encompassing several variants of image retrieval, SFM, and RGBD-based localization techniques relying on robust local and global image features. **Third**, we propose extensive experimental validation of *kapture* as well as the pipeline and its variants on eight challenging visual localization datasets ranking top on all and first on many of them. The *kapture* toolbox, including code and datasets used in this paper (in *kapture* format), is publicly available.

2. Related Work

Local features. Local features play an important role in visual localization as shown in recent benchmarks comparing local features for matching [15, 48], SFM [96], and localization [42, 48]. Early methods used handcrafted local feature extractors, notably the popular SIFT descriptor [65]. However, such keypoint extractors and descriptors have several limitations, including the fact that they are not necessary tailored to the challenges of the target task, in particular to changing conditions such as day-night and seasons of the year. Therefore, several data-driven learned representations were proposed recently including learning local features with end-to-end deep architectures (see the evolution of local features in [29, 96]). In particular, Key.Net [18] has shown state-of-the-art keypoint detection performance, SuperGlue [83] and AdaLAM [25] improve feature matching, while the joint detector+descriptors Superpoint [33], D2-Net [36], R2D2 [80], and ASLFeat [66] report state-of-the-art performance on several local feature and visual localization benchmarks [15, 48, 42].

In this paper we use R2D2, D2-Net, ASLFeat, and SIFT for local feature matching. We also propose a modification of the R2D2 network architecture that reduces its processing time by a factor three and preserves or even improves the localization accuracy.

Global image representations. Another key element are global image representations used for image retrieval. Image retrieval-based localization methods [108, 102, 84, 36, 41, 126, 39] mostly use the handcrafted DenseVLAD [105], which aggregates local RootSIFT [10, 65] descriptors extracted on a multi-scale, densely sampled grid into an intra-

normalized VLAD representation [46] or NetVLAD [105], which aggregates mid-level convolutional features extracted from the entire image into a compact single vector representation for efficient indexing in a similar way. [75] compares these features with state-of-the-art deep image representations APGeM [78] and DELG [23] trained on landmark recognition tasks, where the aim is to retrieve images of the same building or place, independently of the pose or viewing conditions. APGeM, similarly to [77] uses a generalized-mean pooling layer (GeM) to aggregate CNN-based descriptors of several image regions at different scales but instead of contrastive loss, it directly optimizes the Average Precision (AP) approximated by histogram binning to make it differentiable. DELG uses a CNN that is trained to jointly extract local and global features. After a common backbone, the model is split into two parts (heads), one to detect relevant local feature and one which describes the global content of the image as a compact descriptor. The two networks are jointly trained in an end-to-end manner using the ArcFace [31] loss for the global descriptor. The method was originally designed for image search, where the local features enable geometric verification and re-ranking.

In this paper, we use DenseVLAD, NetVLAD, APGeM, and DELG for image retrieval. We also propose a late fusion technique [28] to combine multiple global image representations in order to outperform each representation individually.

Datasets and processing. In order to evaluate visual localization methods under various conditions and scenarios, several datasets were introduced. Some relevant examples are Cambridge Landmarks [52], an outdoor dataset consisting of 6 landmarks of the city of Cambridge, UK and 7-scenes [99], which consists of seven small indoor areas captured using an RGBD camera. Furthermore, [91] provides an online benchmark which includes several datasets covering a variety of challenges for visual localization in different application scenarios such as autonomous driving and indoor as well as outdoor handheld camera localization (see Section 4.1 for more details). More examples include TUM-LSI [111], ETH3D [97], KITTI [40], Middlebury [98], and 1DSfM [116].

Next to various datasets, a rich set of tools for visual localization and SFM was released in the last two decades which greatly boosted the research and applications in these fields. While the variety of tools and datasets is important and provides many opportunities, the different data formats they come with impose operational challenges using them in practice. For example, well established tools like Bundler [72], COLMAP [95], OpenMVG [71], OpenSfM [68], VisualSfM [117], as well as the datasets mentioned above, all come with their own data format. To better understand the differences, Table 1 compares popular data formats. We mark a data type as supported if it is inher-

Data	Bundler	COLMAP	OpenMVG	OpenSfM	VisualSfM	kapture
Sensor data						
Camera intrinsics	X	X	X	X	X	X
Extrinsics	X	X	X	X	X	X
Camera rig	-	(X)	-	-	-	X
GNSS (GPS)	-	(X) EXIF	(X) EXIF	X	(X) EXIF	X
LiDAR point cloud	-	-	-	-	-	X
Depth map	-	(X)	-	(X)	-	X
Other sensors	-	-	-	-	-	X
Reconstruction data						
Local features	X	X	X	X	(X)	X
Global features	-	-	-	-	-	X
Matches	X	X	X	X	X	X
Observations	X	X	X	X	X	X
3D points	X	X	X	X	X	X

Table 1. Comparison of various SFM tools and data formats. X: supported, (X): partly supported, -: not supported

ently part of the format and not only a product of a processing step. For example, COLMAP can produce depth maps from reconstructions but it is not possible to import depth data from an RGBD camera. As can be seen, none of them fulfills all requirements of modern visual and sensor-based localization (see Section 3 for details). Notably, none of the existing data formats supports global features, 3D sensor data (e.g. LiDAR or RGBD), and integration of other sensors such as WiFi or IMU (inertial measurement unit). Extending an existing format would be a valid option (and is often done in practice), however this would disentangle it from its original purpose which we think will not have great usability and impact. Thus, inspired by existing formats and practical needs, we decided to design a new data format from scratch that combines all required features, is extendable and independent of existing tools but easily convertible into existing data formats.

The remainder of the paper is structured as follows. First, in Section 3, we introduce and describe our new toolbox kapture. Second, in Section 3.1, we describe our mapping and localization pipeline and its variants. Finally, in Section 4, we show extensive experimental evaluations and comparisons that highlight the versatility of kapture and provide interesting insights on visual localization using different datasets.

3. Kapture description

As briefly summarized in Figure 1, kapture consists of the following core features we think are essential for modern visual localization¹.

Sensor data. The minimum data needed for visual localization are images as well as intrinsic and extrinsic camera parameters (supporting various camera and image distortion models). If multiple cameras are used, their data should be associated with timestamps and the relative transformations between these cameras should be provided. This allows to define static, ideally time-synchronized, camera rigs and the usage of image sequences (Section 4.1 presents examples for both). Furthermore, modern location-based services not

¹A full format specification and API is provided on the kapture website.

only use images for localization but rather combine visual localization with data coming from other sensors such as WiFi [43], GNSS [5], or IMUs [50]. Finally, self-driving cars or mobile robot platforms are often equipped with 3D sensors such as Lidar scanners [30] or RGBD cameras [6]. The kapture format supports all of this and provides a clear definition of cameras, sensors, and their respective parameters.

Reconstruction data. Another important aspect is handling processed data such as local and global image features, keypoint matches, keypoint observations, 3D points, and image lists that contain image pairs to be matched. The kapture format unifies the definition of such data.

Processing tools. Since kapture is designed to facilitate the use of existing and future open source tools and datasets, it consists of a growing set of conversion tools between existing formats. kapture also contains tools to perform the entire visual localization pipeline presented in this paper. Finally, kapture provides tools to merge, split, comparing, and evaluate datasets.

Datasets. kapture is not only a data format definition, we also provide all datasets used in this paper for download using a first of its kind dataset downloader (included in the toolbox).

Open source. In an effort to ease further research in the field, we publicly release kapture. We believe that it will facilitate large-scale experiments with a multitude of datasets, it will provide new opportunities to combine existing tools, and it will unveil new directions for benchmarking, visual localization and SFM research, as well as sensor fusion.

3.1. Mapping and localization pipeline

In order to demonstrate the versatility of kapture, we implemented and evaluated a structure-based localization pipeline (Figure 3) utilizing images, camera poses, and depth maps. We follow the workflow of image retrieval as well as structure-based methods for mapping (Figure 2) and localization (Figure 3). For image retrieval, we use multiple global image representations (Section 4.3), for local feature matching, we use state-of-the-art methods such as R2D2 [79], SIFT [65], D2-Net [36], and ASLFeat [66] (Section 4.2). For 3D point triangulation (e.g. during mapping), we use the COLMAP SFM library [95]. For image registration, we again use COLMAP, but also RansacLib [86, 60], and pycolmap [35]. We compare these variants in Section 4.4 and use COLMAP as default configuration for all other experiments.

Mapping. We use two strategies to generate 3D maps, SFM and RGBD. SFM is one of the most popular strategies for reconstruction of a 3D scene from un-ordered photo collections [100, 44, 95, 74] and is often used to create 3D models used for visual localization. Figure 2 (top) illus-

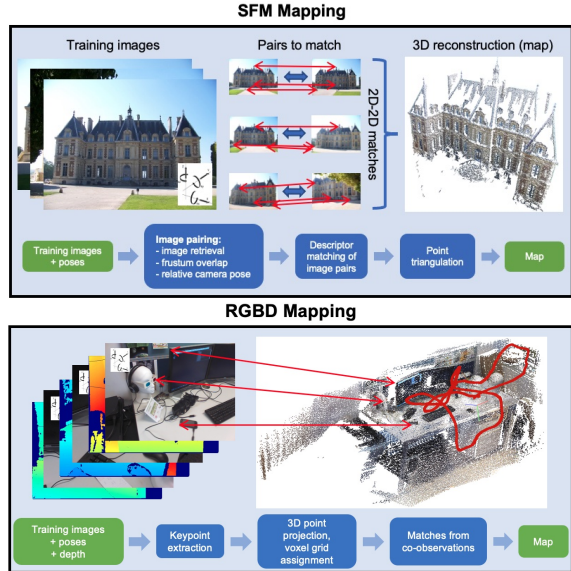


Figure 2. SFM and RGBD mapping pipelines. Image credit: 7-scenes [99] and Sceaux Castle image dataset [71].

trates our approach where we first establish 2D-2D correspondences between local image features (keypoints) of image pairs, followed by geometric verification to remove outliers. By exploiting transitivity, observations of a keypoint found in several images allow to apply relative pose estimation for initialization of the reconstruction followed by 3D point triangulation [49] and image registration for accurate 6DOF camera pose estimation. RANSAC [38, 26, 60] can be used to increase robustness of several steps in this pipeline and bundle adjustment [109] can be used for global (and local) optimization of the model (3D points and camera poses). Note that the visual localization datasets we use in this paper already provide camera poses for the training images, thus, we can skip the camera pose estimation of SFM and directly triangulate the 3D points from the keypoint matches. Since matching all possible training image pairs of a dataset becomes very processing time intensive, we use several strategies (see Figure 2) to create a short list of images to match. *Image retrieval* uses global image features to pair visually similar images, *frustum overlap* pairs images by the size of their overlapping camera frusta, and *relative camera pose* uses the position and orientation difference between cameras to select images that potentially observe the same scene. Note that kapture also provides a pairing scheme that uses co-observations of 3D points obtained from a pre-constructed SFM map.

When RGBD data (e.g. depth maps) is available, as illustrated in Figure 2 (bottom), instead of triangulating keypoint matches, we construct the 3D map by projecting the keypoints to 3D space using the provided depth. If needed, co-observations of the same 3D point can be used to create keypoint correspondences across multiple images.

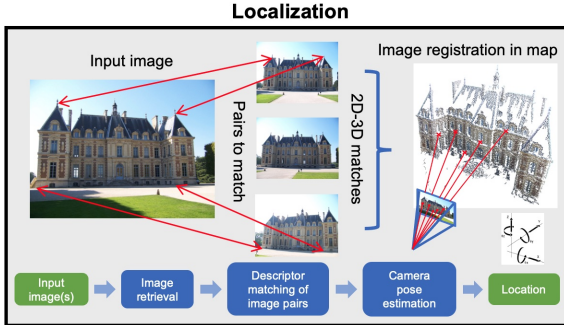


Figure 3. Localization pipeline. Image credit: Sceaux Castle image dataset [71].

Localization. Our localization method (Figure 3), similarly to mapping, establishes 2D-2D local feature correspondences between the query image and the database images used to generate the map. In order to only match relevant images, we use image retrieval to obtain the top k most similar images from the database (we found that $k = 20$ was in general a good choice). Since many keypoints from the database images correspond to 3D points of the map, 2D-3D correspondences between query image and map can be established. These 2D-3D matches are then used to compute the 6DOF camera pose by solving a PNP problem [54, 55, 58] robustly inside a RANSAC loop [38, 26, 60].

4. Experiments

In this section, we present a thorough evaluation of the proposed pipeline and methods. First, we present the evaluation protocol and the datasets used (Section 4.1). Second, we compare visual localization performance of four state-of-the-art local feature types (Section 4.2) and four state-of-the-art global image representations as well as late fusion strategies to combine them (Section 4.3). Third, we present results obtained with different variants of our structure-based pipeline (Section 4.4). Fourth, we show how to leverage image sequences as well as camera rigs for visual localization (Section 4.5). Fifth, we compare our SFM-based mapping method with our RGBD-based approach (Section 4.6). Finally, we compare the best configurations of our pipeline with other top performing state-of-the-art methods on all datasets used in this paper. In order to improve readability, in this section, we only present a summary of the results that best show the versatility and impact of capture. More results can be found in Appendix C.

4.1. Protocol and datasets

For all experiments, we followed our mapping and localization pipelines described in Section 3.1. Since, among others, we use COLMAP in this pipeline, we experimented with multiple parameter sets. Besides the default parameters, **config1**, we found that less strict bundle adjustment

COLMAP image_registrator	config1	config2
--Mapper.ba_refine_focal_length	0	0
--Mapper.ba_refine_principal_point	0	0
--Mapper.ba_refine_extra_params	0	0
--Mapper.min_num_matches	15	4
--Mapper.init_min_num_inliers	100	4
--Mapper.abs_pose_min_num_inliers	30	4
--Mapper.abs_pose_min_inlier_ratio	0.25	0.05
--Mapper.ba_local_max_num_iterations	25	50
--Mapper.abs_pose_max_error	12	20
--Mapper.filter_max_reproj_error	4	12

Table 2. COLMAP parameter configurations used in our experiments.

settings **config2** produce better results for some datasets (see Table 2 for the parameter configuration details). We indicate the used parameters for each experiments, but report the results for the best parameter configuration only.

For evaluation of our methods, we chose the datasets provided by the online visual localization benchmark [42] introduced in [91], which consist of four outdoor datasets, namely Aachen Day-Night v1.1. [91, 93, 122], RobotCar Seasons v2 [91], Extended CMU-Seasons [91, 13], SILDa Weather and Time of Day [14], and one indoor dataset, In-loc [102, 115]. In addition, we use one more popular outdoor dataset, Cambridge Landmarks [52], and three more indoor datasets, 7-scenes [99], Baidu-mall [101], and Gangnam Station B2 [61] for our experiments. As evaluation metric, the five benchmark datasets, Baidu-Mall, and Gangnam Station use the percentage of query images which were localized within three pairs of translation and rotation error thresholds (the thresholds are provided in the respective results tables). Cambridge Landmarks and 7-scenes use the median position and orientation error.

4.2. Local features

Table 3 compares four local features types on our SFM pipeline using image retrieval (top 20) with APGeM [78] features. Next to the features R2D2 [79], D2-Net [36], ASLFeat [66], and SIFT [65], we present results obtained with a modified version of R2D2 that we call Fast-R2D2.

Since the architecture of R2D2 is based on the fully convolutional encoder of L2-net [118], the network will always process the image in its original resolution. While this is a strong asset in the sense that it preserves fine details in the computed features, the computational cost is consequently heavier than that of a more standard convolution+pooling step. In Fast-R2D2, we propose to merge both strategies by taking the R2D2 architecture and adding a single downsampling step inside the network to decrease the computation complexity while staying close to the original image resolution. We restore the input resolution with an upsampling step right before the last convolutions. This modification

Datasets	Algorithm	percentage of successfully localized images							Accuracy thresholds	
Aachen Day-Night v1.1	APGeM-20 config2	avg. all bins	day			night				
	R2D2		high	mid	low	high	mid	low		
	Fast-R2D2	90.32	89.9	96.5	99.5	71.2	86.9	97.9	Accuracy thresholds Aachen high: 0.25m, 2° mid: 0.5m, 5° low: 5m, 10°	
	D2-Net	89.15	85.8	94.3	98.8	70.7	86.9	98.4		
	COLMAP SIFT	79.17	87.7	94.2	98.4	51.8	65.4	77.5		
	ASLFeat	89.97	87.5	95.4	99.3	73.8	85.9	97.9		
RobotCar Seasons v2	APGeM-20 config1 rig seq	avg. all bins	day			night				Accuracy thresholds RobotCar high: 0.25m, 2° mid: 0.5m, 5° low: 5m, 10°
R2D2	79.17		65.7	95.1	100.0	43.6	76.7	93.9		
Fast-R2D2	80.85	65.9	95.1	100.0	46.2	81.4	96.5			
D2-Net	75.65	60.9	93.6	99.9	35.9	72.0	91.6			
COLMAP SIFT	55.97	64.2	92.5	97.9	15.9	27.3	38.0			
ASLFeat	78.98	64.7	94.9	99.9	45.2	77.4	91.8			
Cambridge Landmarks	APGeM-20 config2	avg. all scenes	Great Court	Kings College	Old Hospital	Shop Facade	StMarys Church	Street	Accuracy threshold Cambridge Landmarks 0.5m, 5°	
	R2D2		93.98	86.2	99.7	95.1	99.0	99.4		84.5
	Fast-R2D2	94.43	89.2	99.4	94.5	99.0	99.6	84.9		
	D2-Net	92.30	85.5	99.1	91.2	99.0	99.6	79.4		
	COLMAP SIFT	93.20	85.0	99.4	95.1	99.0	99.4	81.3		
	ASLFeat	93.33	87.9	98.8	92.3	99.0	99.6	82.4		

Table 3. Comparison of different local feature types on three datasets. The learned features R2D2, D2-Net, and ASLFeat often outperform SIFT, notably on difficult night images.

Dataset	Extended-CMU		RobotCar		InLoc train		InLoc test	
Image size	1024x768		1024x1024		1600x1200		4032x3024	
GPU	R2D2	Fast-R2D2	R2D2	Fast-R2D2	R2D2	Fast-R2D2	R2D2	Fast-R2D2
Tesla P40 24GB	1.34	0.46	1.76	0.59	3.28	1.1	15.08	5.43
Tesla V100 32GB	0.57	0.21	0.75	0.27	1.42	0.5	6.75	2.66
Tesla P100 16GB	1.2	0.39	1.58	0.5	2.86	0.9	out-of-mem	4.24

Table 4. Run-time (in seconds) and memory consumption comparison of R2D2 and Fast-R2D2 on four subsets of selected datasets. To minimize data I/O overhead, we did all data processing directly in the computers’ RAM. Note, that for the large images of InLoc test, the 16GB GPU even ran out of memory while running original R2D2.

results in a threefold increase in computation speed and a significantly smaller memory footprint (see Table 4) while, interestingly, achieving slightly better localization performance than the original architecture (Table 3). More details about the architecture of Fast-R2D2 can be found in Appendix A.

The evaluation on three datasets in Table 3 confirms the finding of [79, 36] that learned features often outperform classic SIFT, especially on the night images of Aachen and RobotCar. On Cambridge Landmarks, SIFT performs comparable to R2D2, D2-Net, and ASLFeat.

4.3. Global image representations

In this section, we use our SFM pipeline to compare different global descriptors used for image retrieval. Similar to the experiments in the previous section, we fixed all parameters of the localization pipeline and only changed the image retrieval part. We selected **DenseVLAD** [105] and **NetVLAD** [8], since they were already successfully used for visual localization [105, 92, 94, 84, 41, 36] before, and

we added two new methods, **APGeM** [78] and **DELG** [23] because both methods perform very well on the popular landmark retrieval benchmarks \mathcal{R} Oxford and \mathcal{R} Paris [76]. For our experiments, we used the code and models available at [1, 2, 3, 4].

In addition to these image descriptors, we report results obtained by late fusion of all four of them. Late fusion means that we first compute the similarities for each descriptor individually and then apply a fusion operator. We used the operator *generalized weighted harmonic mean* from [28] (GHARM) for this experiment since it tends to be more robust against outliers than geometric or arithmetic mean. More details about late fusion for image retrieval can be found in Appendix B. Table 5 summarizes the results of our experiments. We see that the learned image descriptors outperform the handcrafted descriptor DenseVLAD on the night images of Aachen and that GHARM consistently outperforms the individual representations. Late fusion, as it is robust to outliers, indeed is interesting to improve robustness and reliability.

Datasets	Algorithm	percentage of successfully localized images									
Aachen Day-Night v1.1	R2D2 top20 config2	avg. all bins	day			night			Accuracy thresholds Aachen Extended-CMU high: 0.25m, 2° mid: 0.5m, 5° low: 5m, 10°		
	APGeM		90.32	89.9	96.5	99.5	71.2	86.9			
	DELG	90.55	90.0	96.0	99.2	73.3	87.4	97.4			
	NetVLAD	90.60	88.7	95.1	98.1	74.3	89.5	97.9			
	DenseVLAD	84.93	88.2	94.2	97.3	62.8	79.1	88.0			
	GHARM	91.68	90.5	96.8	99.4	74.9	90.1	98.4			

Extended-CMU	R2D2 top20 config1 rig seq	avg. all bins	urban			suburban			park		
	APGeM		94.87	96.7	98.9	99.7	94.4	96.8	99.2	83.6	89.0
	DELG	95.00	96.6	98.8	99.7	94.1	96.7	99.1	84.7	89.6	95.7
	NetVLAD	95.94	97.1	99.1	99.8	93.8	96.3	99.1	88.1	92.7	97.5
	DenseVLAD	95.66	96.1	98.4	99.4	94.2	96.7	99.1	87.9	92.3	96.8
	GHARM	96.38	97.0	99.1	99.8	95.0	97.0	99.4	89.2	93.4	97.5

Table 5. Comparison of different global image representations as well as a late fusion strategy on three datasets. The learned descriptors outperform the DenseVLAD on the night images of Aachen and GHARM consistently outperforms the individual representations.

4.4. Pipeline variants

In this section, we present localization results obtained with different image pairing methods as well as different image registration variants using 2D-3D correspondences.

Pairing. We compare the strategies *image retrieval*, *distance*, and *frustum overlap* for image pair selection during the mapping process. For localization, we use APGeM for image retrieval (top 20) and R2D2 for local feature matching. Note that, contrary to the place recognition literature [106, 9, 88], where *distance* is usually used as binary score (an image is relevant if it is below a position and orientation threshold τ_c resp. τ_R), we rank the images using the normalized distance score $s(q, t) = \frac{c_{\text{diff}}}{\tau_c} + \frac{R_{\text{diff}}}{\tau_R}$, where c_{diff} and R_{diff} are computed between the pose of image q ($\mathbf{c}_q, \mathbf{R}_q$) and the pose of image t ($\mathbf{c}_t, \mathbf{R}_t$). The role of τ_c and τ_R is to normalize position distance and angle, making them more comparable. We use $\tau_c = 25m$ and $\tau_R = 45^\circ$ in our experiment. The results on two datasets in Table 6 show that *distance* performs best, followed by image retrieval. This suggests that *distance*, even if it does not take visual content into account and as a consequence might suffer from occlusions, is well suited to generate 3D maps without the need of processing intensive brute force matching or introducing bias by using specific global features.

Image registration. While many algorithms are directly implemented in kapture (e.g. feature extraction, keypoint matching, image pairing, etc.), it also enables the easy use of methods provided in external libraries. To demonstrate this, kapture provides native support for several open source tools (see Section 3), including interfaces to COLMAP [95], Python bindings for pose estimators of COLMAP [35], as well as RansacLib [86, 60, 53], a template-based library that

Datasets	Algorithm	percentage of successfully localized images									
Aachen Day-Night v1.1	R2D2	avg. all bins	day			night			Accuracy thresholds Aachen, Baidu-mall high: 0.25m, 2° mid: 0.5m, 5° low: 5m, 10°		
	APGeM-20		high	mid	low	high	mid	low			
	AP-GeM	90.33	89.4	96.2	99.4	71.7	86.9	98.4			
	distance	90.50	89.4	96.6	99.4	72.3	87.4	97.9			
	frustum	86.28	86.7	84.9	99.0	68.1	83.2	95.8			
Baidu-mall	R2D2	avg. all bins	all			Accuracy thresholds Aachen, Baidu-mall high: 0.25m, 2° mid: 0.5m, 5° low: 5m, 10°					
	APGeM-20		high	mid	low						
	AP-GeM	71.30	57.5	73.4	83.0						
	distance	71.97	58.3	74.2	83.4						
	frustum	71.63	58.6	73.5	82.8						

Table 6. Comparison of different image pairing strategies. Method *distance* performs best, followed by image retrieval. Note that for *image retrieval* we recommend to use the same descriptor as used for localization (APGeM in our experiments). All methods use, if available, the top 20 image pairs.

implements different RANSAC variants.

In this section we use these implementations to compare three variants of image registration that can be used with kapture. The variant COLMAP stands for COLMAP’s image registrator which needs the dataset to be fully converted to COLMAP’s format (e.g. using kapture). Pycolmap allows direct access to COLMAP’s absolute camera pose estimators without the need of data import, and RansacLib provides easy access to multiple RANSAC implementations, also directly accessible from kapture format. Table 7 shows that all variants perform similarly with a small advantage of COLMAP. Note that we did not evaluate the full range of RANSAC implementations of RansacLib but we think that this is an interesting task for future work.

4.5. Camera rigs and image sequences

In order to evaluate how camera rigs and image sequences can be used to improve localization performance, we implemented two post-processing steps applicable for

Datasets	Algorithm	percentage of successfully localized images							Accuracy thresholds
Aachen Day-Night v1.1	R2D2 frustum,APGeM-20	avg. all bins	day			night			
	COLMAP config2		89.8	96.5	99.4	73.3	86.9	97.9	
	pycolmap	90.63	89.9	96.4	99.4	73.8	86.4	97.9	
	ransaclib	90.62	90.1	96.5	99.5	73.3	85.9	98.4	
Gangnam Station B2	R2D2 distance-50,APGeM-20	avg. all bins	test			validation			Gangnam B2 high: 0.1m, 1° mid: 0.25m, 2° low: 1m, 5°
	COLMAP config2		53.35	42.6	60.4	64.8	35.8	56.4	
	pycolmap	55.97	44.3	62.5	66.9	38.1	59.6	64.4	
	ransaclib	56.12	44.5	62.4	67.0	38.7	59.9	64.2	
Baidu-mall	R2D2 frustum,APGeM-20	avg. all bins	all			Accuracy thresholds Baidu-mall high: 0.25m, 2° mid: 0.5m, 5° low: 5m, 10°			
	COLMAP config2		71.77	58.6	73.7				83.0
	pycolmap	72.97	60.0	75.0	83.9				
	ransaclib	73.13	59.9	75.6	83.9				

Table 7. Comparison of different variants of our pipeline. We use APGeM-20 and R2D2 features for all variants. *config2* is a set of relaxed bundle adjustment parameters for COLMAP that allow more images to be localized, even if the individual error is higher.

any localization method and one algorithm that directly uses a multi-camera rig during localization. We evaluated them on RobotCar, Extended-CMU, and SILDa (these datasets provide synchronized camera rigs). RobotCar provides the camera rig calibration (transforms between the cameras) as part of the dataset. For Extended-CMU and SILDa, we estimated it using the training poses.

The first post-processing step (*rig*) uses the camera rig calibration to compute the pose for all images of the rig given one successfully localized camera. The second post-processing step assigns poses to non-localized images within query sequences (defined using timestamps) using linear interpolation between the two closest successfully localized images. If this is not possible, we use the nearest neighbor. Table 8 shows that the highest improvement over the single camera setup can be achieved with the camera rig. Furthermore, utilizing the image sequences gives a little boost for the datasets we used for our experiments.

While these two post-processing methods can be used to spatially and temporally complete not successfully localized images, they do not directly leverage multi-camera rigs. To demonstrate this, we implemented an interface to the generalized P3P (GP3P) [56, 53] implementation of [87, 112], a method that utilizes known relative poses between multiple images for multi-camera pose estimation. We evaluated this method on the RobotCar dataset and observe that it performs better than using only one camera and similarly to using rig and sequence post-processing. This method is useful if, *e.g.*, the individual cameras on a rig do not find enough local feature matches to localize. More investigation of such scenarios is an interesting direction for future work using kapture.

4.6. RGBD-based localization

An accurate 3D representation of the environment is crucial for precise camera localization. So far, in this paper, we constructed the maps by triangulating feature matches using the provided training images and poses. In this section, we show the impact of using depth maps for this step on the RGBD dataset 7-scenes [99]. Figure 4 shows two maps of the same scene, SFM (left) and RGBD (right), where a clear difference in reconstruction quality can be seen: the SFM map is noisier than the RGBD map. We explain this by the fact that the RGBD camera is not calibrated and that the camera poses are not accurate enough for precise keypoint triangulation. Contrary, when directly using depth from a dedicated sensor, the 3D reconstruction depends less on the camera poses (because the 3D points do not come from triangulation), which explains the cleaner map produced by RGBD. Table 9 compares localization performance on these two maps (for both experiments we use APGeM top 20 and R2D2 for localization) confirming this observation. We see a significant improvement in accuracy when using RGBD.

The second RGBD dataset we use in this paper is In-Loc [102, 115] which represents an indoor scenario captured in multiple university buildings (only DUC1 and DUC2 are used here). There is only little overlap between the training images of this dataset which results in an SFM model which is, according to our experience, too sparse for visual localization pipelines. Instead, similarly as described above, we constructed the map using the provided 3D points which results in a very dense 3D reconstruction which can be used for the localization experiments presented in Table 10. We are convinced that kapture will enable more research on RGBD-based localization in the future.

Datasets	Algorithm	Rig and sequence post-processing, percentage of localized images							
RobotCar Seasons v2	R2D2 APGeM top20 config1	avg. all bins	day			night			Accuracy thresholds high: 0.25m, 2° mid: 0.5m, 5° low: 5m, 10°
	rig + seq		79.17	65.7	95.1	100	43.6	76.7	
	rig	77.85	65.7	95.1	100	43.6	76	86.7	
	none	76.25	65.7	95.1	99.9	41.5	73	82.3	
	pycolmap rig	79.70	61.8	94.6	100	48.0	81.6	92.2	
	multicamerapose	79.28	61.1	94.5	100	49.0	80.7	90.4	

Extended- CMU	R2D2 APGeM top20 config1	avg. all bins	urban			suburban			park		
	rig + seq		94.87	96.7	98.9	99.7	94.4	96.8	99.2	83.6	89
	rig	94.30	96.5	98.8	99.5	94.3	96.7	99.1	83.1	87.9	92.8
	none	89.11	95.8	98.1	98.8	88.9	91.1	93.4	75.5	78.4	82

SILDa Weather and Time of Day	R2D2 APGeM top20 config1	avg. all bins	evening			snow			night		
	rig + seq		49.97	31.9	66.6	92.5	0.5	5.8	89.2	30.5	54.2
	rig	49.97	31.9	66.6	92.5	0.5	5.8	89.2	30.5	54.2	78.5
	none	46.39	31.8	66.3	89.4	0.3	3.9	64.9	30	53.4	77.5
	pycolmap rig	53.17	37.0	71.0	93.4	2.4	16.4	91.1	32.9	54.6	79.7

Table 8. Evaluation of rig and image sequence post-processing on three datasets. *config1* is the default set of COLMAP parameters that result in accurate poses but might not be able to localize all images. We complete those with *seq* and *rig*.

Method	7-scenes, percentage of successfully localized images (0.05m, 5.0°)							
	avg. all scenes	chess	fire	heads	office	pumpkin	stairs	redkitchen
SFM	66.11	89.6	83.6	92.4	67.9	44.5	36.8	48.0
RGBD	82.47	96.6	94.1	98.1	85.7	62.8	66.2	73.8

Table 9. Comparison of SFM and RGBD mapping.



Figure 4. Comparison of the 7-scenes [99] (office) 3D map created by triangulating R2D2 features (left) and by projecting the features to 3D using the provided depth maps.

4.7. Comparison to state-of-the-art

Finally, we compare our pipeline with top performing state-of-the-art methods on eight popular datasets. In Table 10 (datasets from [42]), we see that our methods are top ranked on all datasets (with leading positions on two of them) but InLoc, which is very challenging for image retrieval and local feature matching. The top performing methods on InLoc either leverage semantic and depth cues [37] or benefit from more advanced matching techniques [83]. Table 11 presents results on the Baidu-mall dataset. The baseline results [101] were computed using a map consisting of 3D points created by a Lidar scanner. Still, only using SFM with frustum-based pairing and top 50 DenseVLAD image features, our method outperforms the current state-of-the-art. Table 12 shows a more comprehensive evaluation on 7-scenes [99] and Cambridge Landmarks [52]. We report results of the best performing algorithms in the literature and show that our methods outperform all of them (using RGBD on 7-scenes and SFM on Cambridge Landmarks).

5. Conclusion

We present kapture, a new, open, extendable data format and toolbox to facilitate processing and evaluation of visual localization and SFM. To demonstrate kapture, we propose a versatile pipeline that enables research on various aspects of visual localization. We evaluate localization performance using multiple global and local feature types, using different variants for image registration, using multi-camera rigs as well as sequence processing for spacial and temporal fusion, and we show how depth data can be used to improve localization. We present a modified version of R2D2 that is three times faster than the original version and increases localization performance on most datasets. Furthermore, we show that late fusion of image representation consistently outperforms image retrieval using individual image descriptors. Finally, our method ranks among the best methods on all datasets used in this paper, defining a new state-of-the-art on five of them. We can con-

Datasets		Algorithm		ours compared to top state-of-the-art methods							
Aachen Day-Night v1.1		avg. all bins	day			night			Accuracy thresholds Aachen high: 0.25m, 2° mid: 0.5m, 5° low: 5m, 10°		
	ours (R2D2 40k,GHARM-50)	92.45	high	mid	low	high	mid	low			
	hloc+SuperGlue [83]	92.15	89.8	96.1	99.4	77.0	90.6	100.0			
	ours (Fast-R2D2,GHARM-20)	91.75	90.3	96.6	99.6	74.9	90.1	99.0			
	RLOCS_v1.0 [37]	89.90	86.0	94.8	98.8	72.3	88.5	99.0			
InLoc		avg all bins	DUC1			DUC2			Accuracy thresholds InLoc high: 0.25m, 10° mid: 0.5m, 10° low: 1m, 10°		
	RLOCS_v1.0 [37]	70.10	high	mid	low	high	mid	low			
	hloc+SuperGlue [83]	68.57	49.0	68.7	80.8	53.4	77.1	82.4			
	ours (Fast-R2D2,RGBD, GHARM-50)	59.55	40.4	63.1	78.3	42.7	64.9	67.9			
	DensePV+S (w/ scan-graph) [103]	58.62	40.9	63.6	71.7	42.7	61.8	71.0			
	InLoc [102]	54.80	40.9	58.1	70.2	35.9	54.2	69.5			
RobotCar Seasons v2		avg all bins	day			night			Accuracy thresholds others high: 0.25m, 2° mid: 0.5m, 5° low: 5m, 10°		
	ours (Fast-R2D2,APGeM-20,rig+seq)	80.85	high	mid	low	high	mid	low			
	hloc+SuperGlue [83]	80.77	63.8	95.0	100.0	45.0	86.2	94.6			
	ours (Fast-R2D2,GHARM-20,rig+seq)	80.17	65.9	95.1	100.0	45.2	80.4	94.4			
Extended- CMU		avg all bins	urban			suburban			park		
	FGSN [57]	98.98	high	mid	low	high	mid	low	high	mid	low
	hloc+SuperGlue [83]	98.38	98.1	99.8	99.9	98.3	99.5	100.0	94.2	97.1	98.5
	ours (R2D2,GHARM-20,rig+seq)	96.87	97.3	99.4	99.8	95.6	97.2	99.4	90.8	94.6	97.7
	Active Search v1.1 [90]	70.48	81.0	87.3	92.4	62.6	70.9	81.0	45.5	51.6	62.0
SILDa Weather and Time of Day		avg all bins	evening			snow			night		
	hloc+SuperGlue [83]	51.59	high	mid	low	high	mid	low	high	mid	low
	ours (R2D2,GHARM-20,rig+seq)	50.22	32.4	67.4	93.3	0.2	4.1	88.9	30.4	54.2	81.1
	NetVLAD (top50) D2-Net [36]	49.33	29.6	67.8	94.8	6.0	16.4	72.3	25.6	51.6	79.9
	ours (Fast-R2D2,GHARM-20,rig+seq)	49.18	28.9	65.9	92.3	0.2	3.4	89.7	28.6	53.4	80.2

Table 10. Comparison of our methods with top performing state-of-the-art methods on the datasets from [42]. Our methods are top ranked on most of them.

Method	% localized (1m, 5.0°)
ours (R2D2,frustum,DenseVLAD-50)	85.0
RootSIFT + VVS	84.8
Direct Matching	83.3
COV + RootSIFT	75.4

Table 11. Comparison of our method with top performing state-of-the-art methods on the Baidu-Mall dataset. All baseline results were taken from [101] and, contrary to ours, computed using a Lidar map.

clude that a combination of robust global (*e.g.* APGeM) and local (*e.g.* R2D2) features is a good choice for visual localization on a large variety of application scenarios. The kapture toolbox, all datasets used converted to kapture format, as well as the presented algorithms are publicly released at github.com/naver/kapture and github.com/naver/kapture-localization.

References

- [1] <http://www.ok.ctrl.titech.ac.jp/~torii/project/247/>. 6
- [2] <https://github.com/Relja/netvlad>. 6
- [3] <https://github.com/naver/deep-image-retrieval>. 6
- [4] <https://github.com/tensorflow/models/tree/master/research/delf/delf/python/delg>. 6
- [5] Google live view. <https://arvr.google.com/ar/>. 4
- [6] Roomba 980. <https://www.irobot.com>. 4
- [7] Julien Ah-Pine, Stéphane Clinchant, Gabriela Csurka, Florent Perronnin, and Jean-Michel Renders. Leveraging Image, Text and Cross-media Similarities for Diversity-focused Multimedia Retrieval. In Henning Müller, Paul Clough, Thomas Deselaers, and Barbara Caputo, editors, *ImageCLEF: Experimental Evaluation in Visual Information Retrieval*, volume 32 of *INRE*, pages 315–342. Springer, 2010. 16
- [8] Relja Arandjelović, Petr Gronát, Akihiko Torii, Tomáš Pajdla, and Josef Sivic. NetVLAD: CNN Architecture for Weakly Supervised Place Recognition. In *CVPR*, 2016. 2, 6
- [9] Relja Arandjelović, Josef Sivic, Masatoshi Okutomi, and Tomáš Pajdla. Dislocation: Scalable Descriptor Distinctiveness for Location Recognition. In *ACCV*, 2014. 7

Datasets	Method	Median 6D Localization Errors					
		Great Court	K. College	Old Hospital	Shop Facade	St M. Church	Street
Cambridge Landmarks	PoseNet [51]	7.00m, 3.7°	0.99m, 1.1°	2.17m, 2.9°	1.05m, 4.0°	1.49m, 3.4°	20.7m, 25.7°
	ActiveSearch [90]	0.24m, 0.1°	0.13m, 0.2°	0.20m, 0.4°	0.04m, 0.2°	0.08m, 0.3°	N/A
	InLoc [102]	1.20m, 0.6°	0.46m, 0.8°	0.48m, 1.0°	0.11m, 0.5°	0.18m, 0.6°	N/A
	DSAC++ [19]	0.40m, 0.2°	0.18m, 0.3°	0.20m, 0.3°	0.06m, 0.3°	0.13m, 0.4°	-
	DSAC* [21]	0.49m, 0.3°	0.15m, 0.3°	0.21m, 0.4°	0.05m, 0.3°	0.13m, 0.4°	-
	HACNet [62]	0.28m, 0.2°	0.18m, 0.3°	0.19m, 0.3°	0.06m, 0.3°	0.09m, 0.3°	N/A
	PixLoc [85]	0.30m, 0.1°	0.14m, 0.2°	0.16m, 0.3°	0.05m, 0.2°	0.10m, 0.3°	N/A
	hloc + SuperGlue [83]	0.16m, 0.1°	0.12m, 0.2°	0.15m, 0.3°	0.04m, 0.2°	0.07m, 0.2°	N/A
	ours (R2D2,APGeM-20)	0.10m, 0.0°	0.05m, 0.1°	0.09m, 0.2°	0.02m, 0.1°	0.03m, 0.1°	0.10m, 0.3°

7-Scenes		Chess	Fire	Heads	Office	Pumpkin	Stairs	Kitchen
	PoseNet [51]	0.13m, 4.5°	0.27m, 11.3°	0.17m, 13.0°	0.19m, 5.6°	0.26m, 4.8°	0.35m, 12.4°	0.23m, 5.4°
	ActiveSearch [90]	0.03m, 0.9°	0.02m, 1.0°	0.01m, 0.8°	0.04m, 1.2°	0.07m, 1.7°	0.04m, 1.0°	0.05m, 1.7°
	InLoc [102]	0.03m, 1.1°	0.03m, 1.1°	0.02m, 1.2°	0.03m, 1.1°	0.05m, 1.6°	0.09m, 2.5°	0.04m, 1.3°
	DSAC++ [19]	0.02m, 0.5°	0.02m, 0.9°	0.01m, 0.8°	0.03m, 0.7°	0.04m, 1.1°	0.09m, 2.6°	0.04m, 1.1°
	HACNet [62]	0.02m, 0.7°	0.02m, 0.9°	0.01m, 0.9°	0.03m, 0.8°	0.04m, 1.0°	0.03m, 0.8°	0.04m, 1.2°
	PixLoc [85]	0.02m, 0.8°	0.02m, 0.7°	0.01m, 0.8°	0.03m, 0.8°	0.04m, 1.2°	0.05m, 1.3°	0.03m, 1.2°
	hloc + SuperGlue [83]	0.02m, 0.9°	0.02m, 0.9°	0.01m, 0.8°	0.03m, 0.9°	0.05m, 1.3°	0.05m, 1.5°	0.04m, 1.4°
	ours (R2D2,RGBD,APGeM-20)	0.02m, 0.8°	0.02m, 0.8°	0.01m, 0.7°	0.03m, 0.8°	0.04m, 1.1°	0.04m, 1.1°	0.03m, 1.1°

Table 12. Comparison of our methods with top performing state-of-the-art methods on 7-scenes [99] and Cambridge Landmarks [52]. Our methods defines a new state-of-the-art on both.

- [10] Relja Arandjelović and Andrew Zisserman. Three Things Everyone Should Know to Improve Object Retrieval. In *CVPR*, 2012. 2
- [11] Shervin Ardehshir, Amir Roshan Zamir, Alejandro Torroella, and Mubarak Shah. Gis-assisted object detection and geospatial localization. In *European Conference on Computer Vision*, pages 602–617. Springer, 2014. 2
- [12] Clemens Arth, Daniel Wagner, Manfred Klopschitz, Arnold Irschara, and Dieter Schmalstieg. Wide Area Localization on Mobile Phones. In *ISMAR*, 2009. 1
- [13] Hernan Badino, Daniel Huber, and Takeo Kanade. The CMU Visual Localization Data Set. <http://3dvis.ri.cmu.edu/data-sets/localization>, 2011. 5, 18
- [14] Vasileios Balntas, Duncan Frost, Rigas Kouskouridas, Axel Barroso-Laguna, Arjang Talattof, Huub Heijnen, and Krystian Mikołajczyk. Silda: Scape imperial localisation dataset, 2019. 5, 19
- [15] Vassileios Balntas, Karel Lenc, Andrea Vedaldi, and Krystian Mikołajczyk. HPatches: a Benchmark and Evaluation of Handcrafted and Learned Local Descriptors. In *CVPR*, 2017. 2
- [16] Vassileios Balntas, Shuda Li, and Victor Prisacariu. ReLocNet: Continuous Metric Learning Relocalisation Using Neural Nets. In *ECCV*, 2018. 2
- [17] Daniel Barath, Michal Polic, Wolfgang Förstner, Torsten Sattler, Tomás Pajdla, and Zuzana Kukelova. Making affine correspondences work in camera geometry computation. In *ECCV*, 2020. 1
- [18] Axel Barroso-Laguna, Edgar Riba, Daniel Ponsa, and Krystian Mikołajczyk. Key.Net: Keypoint Detection by Handcrafted and Learned CNN Filters. In *ICCV*, 2019. 2
- [19] Eric Brachmann and Carsten Rother. Learning Less Is More - 6D Camera Localization via 3D Surface Regression. In *CVPR*, 2018. 1, 11, 20
- [20] Eric Brachmann and Carsten Rother. Expert sample consensus applied to camera re-localization. In *ICCV*, 2019. 1
- [21] Eric Brachmann and Carsten Rother. Visual camera re-localization from rgb and rgb-d images using dsac, 2020. 1, 11, 20
- [22] Mai Bui, Tolga Birdal, Haowen Deng, Shadi Albarqouni, Leonidas J. Guibas, Slobodan Ilic, and Nassir Navab. 6d camera relocalization in ambiguous scenes via continuous multimodal inference. In *ECCV*, 2020. 2
- [23] Bingyi Cao, André Araujo, and Jack Sim. Unifying Deep Local and Global Features for Efficient Image Search. *arXiv*, 2001.05027, 2020. 3, 6
- [24] Tommaso Cavallari, Stuart Golodetz, Nicholas A. Lord, Julien Valentin, Victor A. Prisacariu, Luigi Di Stefano, and Philip H. S. Torr. Real-time rgb-d camera pose estimation in novel scenes using a relocalisation cascade. *PAMI*, 42(10):2465–2477, Oct 2020. 20
- [25] Cavalli, Luca and Larsson, Viktor and Oswald, Martin Ralf, and Sattler, Torsten and Pollefeys, Marc. AdaLAM: Revisiting Handcrafted Outlier Detection. Number *arXiv*:2006.04250, 2020. 2
- [26] Ondřej Chum and Jiří Matas. Optimal randomized ransac. *PAMI*. 1, 4, 5
- [27] Andrea Cohen, Johannes L. Schönberger, Pablo Speciale, Torsten Sattler, Jan-Michael Frahm, and Marc Pollefeys. Indoor-outdoor 3d reconstruction alignment. In *ECCV*. Springer, 2016. 2
- [28] Gabriela Csurka and Stephane Clinchant. An empirical study of fusion operators for multimodal image retrieval. In *2012 10th International Workshop on Content-Based Multimedia Indexing (CBMI)*. 3, 6, 16
- [29] Gabriela Csurka, Christopher R. Dance, and Martin Humenberger. From Handcrafted to Deep Local Invariant Features. *arXiv*, 1807.10254, 2018. 2

- [30] César Debeunne and Damien Vivet. A review of visual-lidar fusion based simultaneous localization and mapping. *Sensors*, 2020. 4
- [31] Jiankang Deng, Jia Guo, and Stefanos Zafeiriou. Arcface: Additive angular margin loss for deep face recognition. 01 2018. 3
- [32] Adrien Depeursinge and Henning Müller. Fusion Techniques for Combining Textual and Visual Information Retrieval. In Henning Müller, Paul Clough, Thomas Deselaers, and Barbara Caputo, editors, *ImageCLEF: Experimental Evaluation in Visual Information Retrieval*, volume 32 of *INRE*. Springer, 2010. 16
- [33] Daniel DeTone, Tomasz Malisiewicz, and Andrew Rabinovich. Superpoint: Self-supervised Interest Point Detection and Description. In *CVPR*, 2018. 2, 15
- [34] Mingyu Ding, Zhe Wang, Jiankai Sun, Jianping Shi, and Ping Luo. CamNet: Coarse-to-Fine Retrieval for Camera Re-Localization. In *ICCV*, 2019. 2
- [35] Mihai Dusmanu et al. Python bindings for COLMAP estimators, 2020. 4, 7
- [36] Mihai Dusmanu, Ignacio Rocco, Tomas Pajdla, Marc Pollefeys, Josef Sivic, Akihiko Torii, and Torsten Sattler. D2-Net: a Trainable CNN for Joint Description and Detection of Local Features. In *CVPR*, 2019. 2, 4, 5, 6, 10, 18, 19
- [37] Huanhuan Fan, Yuhao Zhou, Ang Li, Shuang Gao, Jijun Li, and Yandong Guo. Visual localization using semantic segmentation and depth prediction. *arXiv preprint arXiv:2005.11922*, 2020. 2, 9, 10, 17
- [38] M. Fischler and R. Bolles. Random Sampling Consensus: A Paradigm for Model Fitting with Application to Image Analysis and Automated Cartography. *Communications of the ACM*, 24:381–395, 1981. 1, 4, 5
- [39] Yixiao Ge, Haibo Wang, Feng Zhu, Rui Zhao, and Hongsheng Li. Self-supervising fine-grained region similarities for large-scale image localization. In *ECCV*, 2020. 2
- [40] Andreas Geiger, Philip Lenz, Christoph Stiller, and Raquel Urtasun. Vision meets robotics: The kitti dataset. *International Journal of Robotics Research (IJRR)*, 2013. 3
- [41] Hugo Germain, Guillaume Bourmaud, and Vincent Lepetit. Sparse-to-Dense Hypercolumn Matching for Long-Term Visual Localization. In *International Conference on 3D Vision (3DV)*, 2019. 2, 6
- [42] Lars Hammarstrand, Fredrik Kahl, Will Maddern, Tomas Pajdla, Marc Pollefeys, Torsten Sattler, Josef Sivic, Erik Stenborg, Carl Toft, and Akihiko Torii. Long-Term Visual Localization Benchmark. <https://www.visuallocalization.net/>. 2, 5, 9, 10
- [43] Zakieh S. Hashemifar, Charuvahan Adhivarahan, Anand Balakrishnan, and Karthik Dantu. Augmenting visual SLAM with wi-fi sensing for indoor applications. *Auton. Robots*, 2019. 4
- [44] J. Heinly, J. L. Schönberger, E. Dunn, and J. M. Frahm. Reconstructing the world* in six days. In *CVPR*, 2015. 4
- [45] Lionel Heng, Benjamin Choi, Zhaopeng Cui, Marcel Gepfert, Sixing Hu, Benson Kuan, Peidong Liu, Rang Nguyen, Ye Chuan Yeo, Andreas Geiger, Gim Hee Lee, Marc Pollefeys, and Torsten Sattler. Project AutoVision: Localization and 3D Scene Perception for an Autonomous Vehicle with a Multi-Camera System. In *ICRA*, 2019. 1
- [46] Hervé Jégou, Matthijs Douze, Cordelia Schmid, and Patrick Pérez. Aggregating Local Descriptors Into a Compact Image Representation. In *CVPR*, 2010. 3
- [47] Hervé Jégou, Cordelia Schmid, Hedi Harzallah, and Jakob Verbeek. Accurate Image Search using the Contextual Dissimilarity Measure. *PAMI*, 32(1):2–11, 2010. 16
- [48] Yuhe Jin, Dmytro Mishkin, Anastasiia Mishchuk, Jiří Matas, Pascal Fua, Kwang Moo Yi, and Eduard Trulls. Image Matching across Wide Baselines: From Paper to Practice. *IJCV*, 2020. 2
- [49] Lai Kang, Lingda Wu, , and Yee-Hong Yang. Robust multi-view L2 triangulation via optimal inlier selection and 3D structure refinement. *PR*, 47(9):2974–2992, 2014. 4
- [50] Jonathan Kelly and Gaurav S. Sukhatme. Visual-inertial simultaneous localization, mapping and sensor-to-sensor self-calibration. In *CIRA*, 2009. 4
- [51] Alex Kendall and Roberto Cipolla. Geometric loss functions for camera pose regression with deep learning. In *CVPR*, 2017. 2, 11, 20
- [52] Alex Kendall, Matthew Grimes, and Roberto Cipolla. PoseNet: a Convolutional Network for Real-Time 6-DOF Camera Relocalization. In *ICCV*, 2015. 2, 3, 5, 9, 11, 20
- [53] Laurent Kneip and Paul Furgale. Opengv: A unified and generalized approach to real-time calibrated geometric vision. In *2014 IEEE International Conference on Robotics and Automation (ICRA)*, pages 1–8. IEEE, 2014. 7, 8
- [54] Laurent Kneip, Davide Scaramuzza, and Roland Siegwart. A Novel Parametrization of the Perspective-three-point Problem for a Direct Computation of Absolute Camera Position and Orientation. In *CVPR*, 2011. 1, 5
- [55] Z. Kukulova, M. Bujnak, and T. Pajdla. Real-Time Solution to the Absolute Pose Problem with Unknown Radial Distortion and Focal Length. In *ICCV*, 2013. 5
- [56] Zuzana Kukulova, Jan Heller, and Andrew Fitzgibbon. Efficient intersection of three quadrics and applications in computer vision. In *The IEEE Conference on Computer Vision and Pattern Recognition (CVPR)*, 2016. 8
- [57] Mans Larsson, Erik Stenborg, Carl Toft, Lars Hammarstrand, Torsten Sattler, and Fredrik Kahl. Fine-grained segmentation networks: Self-supervised segmentation for improved long-term visual localization. In *Proceedings of the IEEE International Conference on Computer Vision*, pages 31–41, 2019. 10, 18
- [58] Viktor Larsson, Zuzana Kukulova, and Yinqiang Zheng. Making Minimal Solvers for Absolute Pose Estimation Compact and Robust. In *ICCV*, 2017. 5
- [59] Zakaria Laskar, Iaroslav Melekhov, Surya Kalia, and Juho Kannala. Camera Relocalization by Computing Pairwise Relative Poses Using Convolutional Neural Network. 2017. 2
- [60] Karel Lebeda, Jiri Matas, and Ondrej Chum. Fixing the Locally Optimized RANSAC. In *BMVC*, 2012. 1, 4, 5, 7
- [61] Donghwan Lee, Soohyun Ryu, Suyong Yeon, Yonghan Lee, Deokhwa Kim, Cheolho Han, Yohann Cabon, Philippe

- Weinzaepfel, Nicolas Guerin, Gabriela Csurka, and Martin Humenberger. Large-Scale Localization Datasets in Crowded Indoor Spaces. In *CVPR*, 2021. 5, 20
- [62] Xiaotian Li, Shuzhe Wang, Yi Zhao, Jakob Verbeek, and Juho Kannala. Hierarchical scene coordinate classification and regression for visual localization. In *IEEE/CVF Conference on Computer Vision and Pattern Recognition (CVPR)*, June 2020. 1, 11, 20
- [63] Hyon Lim, Sudipta N. Sinha, Michael F. Cohen, Matt Uyttendaele, and H. Jin Kim. Real-time Monocular Image-based 6-DoF Localization. *IJRR*, 34(4-5):476-492, 2015. 1
- [64] Liu Liu, Hongdong Li, and Yuchao Dai. Efficient Global 2D-3D Matching for Camera Localization in a Large-Scale 3D Map. In *ICCV*, 2017. 1
- [65] David G. Lowe. Distinctive Image Features from Scale-invariant Keypoints. *IJCV*, 60(2):91-110, 2004. 2, 4, 5
- [66] Zixin Luo, Lei Zhou, Xuyang Bai, Hongkai Chen, Jiahui Zhang, Yao Yao, Shiwei Li, Tian Fang, and Long Quan. Aslfeat: Learning local features of accurate shape and localization. In *CVPR*, 2020. 2, 4, 5, 17, 18
- [67] Simon Lynen, Torsten Sattler, Michael Bosse, Joel Hesch, Marc Pollefeys, and Roland Siegwart. Get out of my Lab: Large-scale, Real-Time Visual-Inertial Localization. In *RSS*, 2015. 1
- [68] Mapillary. OpenSfM. <https://www.opensfm.org/docs/dataset.html>. 3
- [69] Sven Middelberg, Torsten Sattler, Ole Untzelmann, and Leif Kobbelt. Scalable 6-DoF Localization on Mobile Devices. In *ECCV*, 2014. 1
- [70] Pierre Moulon, Pascal Monasse, and Renaud Marlet. Global Fusion of Relative Motions for Robust, Accurate and Scalable Structure from Motion. In *ICCV*, 2013. 1
- [71] Pierre Moulon, Pascal Monasse, Renaud Marlet, and Others. Openmvg. <https://github.com/openMVG/openMVG>. 3, 4, 5
- [72] Noah Snavely, and Steven M. Seitz and Richard Szeliski. Bundler. <https://www.cs.cornell.edu/~snavely/bundler>. 3
- [73] Hyeonwoo Noh, André Araujo, Jack Sim, Tobias Weyand, and Bohyung Han. Large-Scale Image Retrieval with Attentive Deep Local Features. In *ICCV*, 2017. 2
- [74] Onur Özyeşil, Vladislav Voroninski, Ronen Basri, and Amit Singer. A survey of structure from motion. *Acta Numerica*, 26:305-364, 2017. 4
- [75] Noé Pion, Martin Humenberger, Gabriela Csurka, Johann Cabon, and Torsten Sattler. Benchmarking Image Retrieval for Visual Localization. In *3DV*, 2020. 1, 2, 3
- [76] Filip Radenović, Asmet Iscen, Giorgos Tolias, and Ondřej Avrithis, Yannis Chum. Revisiting Oxford and Paris: Large-scale Image Retrieval Benchmarking. In *CVPR*, 2018. 2, 6, 15
- [77] Filip Radenović, Giorgos Tolias, and Ondřej Chum. Fine-Tuning CNN Image Retrieval with no Human Annotation. *PAMI*, 41(7):1655-1668, 2019. 2, 3
- [78] Jérôme Revaud, Jon Almazan, Rafael Sampaio de Rezende, and Cesar Roberto de Souza. Learning with Average Precision: Training Image Retrieval with a Listwise Loss. In *ICCV*, 2019. <https://github.com/naver/deep-image-retrieval>. 2, 3, 5, 6
- [79] Jérôme Revaud, Philippe Weinzaepfel, César De Souza, and Martin Humenberger. R2D2: Reliable and Repeatable Detectors and Descriptors. In *NeurIPS*, 2019. <https://github.com/naver/r2d2>. 2, 4, 5, 6, 15
- [80] Jérôme Revaud, Philippe Weinzaepfel, César De Souza, Noé Pion, Gabriela Csurka, Johann Cabon, and Martin Humenberger. R2D2: Reliable and Repeatable Detectors and Descriptors for Joint Sparse Keypoint Detection and Local Feature Extraction. *CoRR*, (arXiv:1906.06195), 2019. 2
- [81] Jérôme Revaud, Philippe Weinzaepfel, César Roberto de Souza, and Martin Humenberger. R2D2: repeatable and reliable detector and descriptor. In *NeurIPS*, 2019. 15
- [82] Renato F. Salas-Moreno, Richard A Newcombe, Hauke Strasdat, Paul HJ Kelly, and Andrew J Davison. Slam++: Simultaneous localisation and mapping at the level of objects. In *CVPR*, 2013. 2
- [83] Paul-Edouard Sarlin, Daniel DeTone, Tomasz Malisiewicz, and Andrew Rabinovich. SuperGlue: Learning feature matching with graph neural networks. In *CVPR*, 2020. 2, 9, 10, 11, 17, 18, 19, 20
- [84] Paul-Edouard Sarlin, Cesar Cadena, Roland Siegwart, and Marcin Dymczyk. From Coarse to Fine: Robust Hierarchical Localization at Large Scale. In *CVPR*, 2019. 1, 2, 6
- [85] Paul-Edouard Sarlin, Ajaykumar Unagar, Måns Larsson, Hugo Germain, Carl Toft, Viktor Larsson, Marc Pollefeys, Vincent Lepetit, Lars Hammarstrand, Fredrik Kahl, and Torsten Sattler. Back to the feature: Learning robust camera localization from pixels to pose, 2021. 2, 11, 20
- [86] Torsten Sattler et al. RansacLib - A Template-based *SAC Implementation, 2019. 4, 7
- [87] Torsten Sattler et al. Multi Camera Pose Estimation, 2020. 8
- [88] Torsten Sattler, Michal Havlena, Konrad Schindler, and Marc Pollefeys. Large-Scale Location Recognition and the Geometric Burstiness Problem. In *CVPR*, 2016. 7
- [89] T. Sattler, B. Leibe, and L. Kobbelt. Fast image-based localization using direct 2d-to-3d matching. In *ICCV*, 2011. 1
- [90] Torsten Sattler, Bastian Leibe, and Leif Kobbelt. Efficient & Effective Prioritized Matching for Large-Scale Image-Based Localization. *PAMI*, 39(9):1744-1756, 2017. 1, 10, 11, 18, 20
- [91] Torsten Sattler, Will Maddern, Carl Toft, Akihiko Torii, Lars Hammarstrand, Erik Stenborg, Daniel Safari, Masatoshi Okutomi, Marc Pollefeys, Josef Sivic, Fredrik Kahl, and Tomas Pajdla. Benchmarking 6DoF Outdoor Visual Localization in Changing Conditions. In *CVPR*, 2018. 3, 5, 15, 17, 18
- [92] Torsten Sattler, Akihiko Torii, Josef Sivic, Marc Pollefeys, Hajime Taira, Masatoshi Okutomi, and Tomas Pajdla. Are Large-Scale 3D Models Really Necessary for Accurate Visual Localization? In *CVPR*, 2017. 6
- [93] Torsten Sattler, Tobias Weyand, Bastian Leibe, and Leif Kobbelt. Image Retrieval for Image-Based Localization Revisited. In *BMVC*, 2012. 5, 15, 17

- [94] Torsten Sattler, Qunjie Zhou, Marc Pollefeys, and Laura Leal-Taixé. Understanding the Limitations of CNN-based Absolute Camera Pose Regression. In *CVPR*, 2019. 2, 6
- [95] Johannes L. Schönberger and Jan-Michael Frahm. Structure-from-motion Revisited. In *CVPR*, 2016. <https://colmap.github.io>. 1, 3, 4, 7, 16, 17, 18, 19
- [96] Johannes L. Schönberger, Hans Hardmeier, Torsten Sattler, and Marc Pollefeys. Comparative Evaluation of Hand-Crafted and Learned Local Features. In *CVPR*, 2017. 2
- [97] Thomas Schöps, Johannes L. Schönberger, Silvano Galliani, Torsten Sattler, Konrad Schindler, Marc Pollefeys, and Andreas Geiger. A multi-view stereo benchmark with high-resolution images and multi-camera videos. In *CVPR*, 2017. 3
- [98] Steve Seitz, Brian Curless, James Diebel, Daniel Scharstein, and Richard Szeliski. A comparison and evaluation of multi-view stereo reconstruction algorithms. In *cvpr*, 2006. 3
- [99] Jamie Shotton, Ben Glocker, Christopher Zach, Shahram Izadi, Antonio Criminisi, and Andrew Fitzgibbon. Scene Coordinate Regression Forests for Camera Relocalization in RGB-D Images. In *CVPR*, 2013. 1, 3, 4, 5, 8, 9, 11, 20
- [100] N. Snavely, S.M. Seitz, and R. Szeliski. Modeling the World from Internet Photo Collections. *IJCV*, 80(2):189–210, 2008. 4
- [101] Xun Sun, Yuanfan Xie, Pei Luo, and Liang Wang. A Dataset for Benchmarking Image-based Localization. In *CVPR*, 2017. 5, 9, 10, 19
- [102] H. Taira, M. Okutomi, T. Sattler, M. Cimpoi, M. Pollefeys, J. Sivic, T. Pajdla, and A. Torii. InLoc: Indoor Visual Localization with Dense Matching and View Synthesis. *PAMI*, pages 1–1, 2019. 1, 2, 5, 8, 10, 11, 17, 20
- [103] Hajime Taira, Ignacio Rocco, Jiri Sedlar, Masatoshi Okutomi, Josef Sivic, Tomas Pajdla, Torsten Sattler, and Akihiko Torii. Is This the Right Place? Geometric-Semantic Pose Verification for Indoor Visual Localization. In *ICCV*. 10, 17
- [104] Giorgos Toliás, Tomáš Jeníček, and Ondrej Chum. Learning and aggregating deep local descriptors for instance-level recognition. In *ECCV*, 2020. 2
- [105] Akihiko Torii, Relja Arandjelović, Josef Sivic, Masatoshi Okutomi, and Tomáš Pajdla. 24/7 Place Recognition by View Synthesis. In *CVPR*, 2015. 2, 3, 6
- [106] Akihiko Torii, Josef Sivic, Masatoshi Okutomi, and Tomas Pajdla. Visual Place Recognition with Repetitive Structures. *PAMI*, 37(11):2346–2359, 2015. 7
- [107] Akihiko Torii, Josef Sivic, and Tomáš Pajdla. Visual Localization by Linear Combination of Image Descriptors. In *ICCV-W*, 2011. 2
- [108] A. Torii, H. Taira, J. Sivic, M. Pollefeys, M. Okutomi, T. Pajdla, and T. Sattler. Are Large-Scale 3D Models Really Necessary for Accurate Visual Localization? *PAMI*, pages 1–1, 2019. 2
- [109] Bill Triggs, Philip F McLauchlan, Richard I Hartley, and Andrew W Fitzgibbon. Bundle adjustment—a modern synthesis. In *International workshop on vision algorithms*, pages 298–372. Springer, 1999. 4
- [110] J. Valentin, A. Dai, M. Niessner, P. Kohli, P. Torr, S. Izadi, and C. Keskin. Learning to Navigate the Energy Landscape. In *3DV*, 2016. 16, 20
- [111] Florian Walch, Caner Hazirbas, Laura Leal-Taixé, Torsten Sattler, Sebastian Hilsenbeck, and Daniel Cremers. Image-based localization using lstms for structured feature correlation. In *ICCV*, 2017. 3
- [112] Johanna Wald, Torsten Sattler, Stuart Golodetz, Tommaso Cavallari, and Federico Tombari. Beyond Controlled Environments: 3D Camera Re-Localization in Changing Indoor Scenes. In *ECCV*. 8
- [113] Qianqian Wang, XiaoWei Zhou, Bharath Hariharan, and Noah Snavely. Learning feature descriptors using camera pose supervision. In *ECCV*, 2020. 2
- [114] Philippe Weinzaepfel, Gabriela Csurka, Yohann Cabon, and Martin Humenberger. Visual Localization by Learning Objects-Of-Interest Dense Match Regression. In *CVPR*, 2019. 2
- [115] Erik Wijmans and Yasutaka Furukawa. Exploiting 2d floor-plan for building-scale panorama rgbd alignment. In *CVPR*, 2017. 5, 8, 17
- [116] Kyle Wilson and Noah Snavely. Robust global translations with 1dsfm. In *ECCV*, 2014. 3
- [117] Changchang Wu. VisualSFM. <http://ccwu.me/vsfm>. 3
- [118] Tian Yurun, Fan Bin, and Wu Fuchao. L2-net: Deep learning of discriminative patch descriptor in euclidean space. In *CVPR*, 2017. 5, 15
- [119] Amir Roshan Zamir and Mubarak Shah. Accurate Image Localization Based on Google Maps Street View. In *ECCV*, 2010. 2
- [120] Shaoting Zhang, Ming Yang, Timothee Cour, Kai Yu, and Dimitris N. Metaxas. Query Specific Fusion for Image Retrieval. In *ECCV*, 2012. 16
- [121] Wei Zhang and Jana Kosecka. Image Based Localization in Urban Environments. In *International Symposium on 3D Data Processing, Visualization, and Transmission (3DPVT)*, 2006. 2
- [122] Zichao Zhang, Torsten Sattler, and Davide Scaramuzza. Reference Pose Generation for Long-term Visual Localization via Learned Features and View Synthesis. *IJCV*, 2020. 5
- [123] Zichao Zhang, Torsten Sattler, and Davide Scaramuzza. Reference Pose Generation for Visual Localization via Learned Features and View Synthesis. *arXiv*, 2005.05179, 2020. 15, 17
- [124] Enliang Zheng and Changchang Wu. Structure From Motion Using Structure-Less Resection. In *ICCV*, 2015. 2
- [125] Liang Zheng, Shengjin Wang, Lu Tian, Fei He, Ziqiong Liu, and Qi Tian. Query-adaptive Late Fusion for Image Search and Person Re-identification. In *CVPR*, 2015. 16
- [126] Qunjie Zhou, Torsten Sattler, Marc Pollefeys, and Laura Leal-Taixé. To Learn or not to Learn: Visual Localization from Essential Matrices. In *ICRA*, 2020. 2
- [127] Yao Zhou, Guowei Wan, Shenhua Hou, Li Yu, Gang Wang, Xiaofei Rui, and Shiyu Song. DA4AD: end-to-end deep attention-based visual localization for autonomous driving. In *ECCV*, 2020. 1

APPENDIX

In the appendix, we first provide a detailed description of the proposed Fast-R2D2 architecture (Section A) as well as the proposed late fusion techniques (Section B). Second, we present additional experiments that complement the findings we discuss in the main paper (Section C).

A. Fast-R2D2

R2D2 [79] is a sparse keypoint extractor that jointly performs detection and description but separately estimates keypoint reliability and keypoint repeatability. Keypoints with high likelihoods on both aspects are chosen, which improves the overall feature matching pipeline. In this section, we revisit the architecture of the network and present a significantly faster model (see Table 4) that achieves the same order of precision as the original network, thus better suited for practical localization tasks in section A.1. The details of the model training are explained in section A.2 and we present the hyper-parameter search that motivated the chosen architecture in section A.3. The code and models for both R2D2 and Fast-R2D2 can be found at github.com/naver/r2d2.

A.1. Architecture

The core of the architecture is based on the fully convolutional encoder of [118], to which three branches are appended that respectively predict the descriptors, their repeatability, and their reliability. These branches are left as in the original R2D2 paper and we focus here on the core of the network. As described in Figure 6 (top), it consists of a stack of dilated convolution blocks with increasing dilation factors. For the same number of parameters compared to a standard convolution and pooling block, the dilated layer increases the receptive field while preserving the input resolution for maximal detail preservation. However, through the different layers of the network, the depth of the channels increases, and so does the number of floating point operations. Computation time is not problematic for small scale evaluations but hinders applicability in practice for larger scale mapping and localization tasks.

We claim that we can achieve the same level of performances in a much faster fashion. To that aim and similarly to SuperPoint [33], we propose to incorporate an early down-sampling step in the network in the form of a pooling layer, process the lower resolution image, and up-sample the output to the original resolution right before the three branches prediction. At the end, we up-sample the feature map to the input resolution using bi-linear interpolation.

A.2. Training and inference

For the sake of fairness in the comparison, we train our faster architectures using the code of R2D2, with the exact

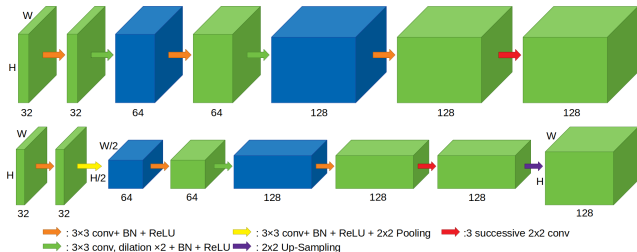


Figure 5. Comparison of the original core architecture [118] (top) and the proposed one (bottom). The three prediction branches (same as in [79]) are omitted for readability.

same training data and losses. Both, the R2D2 and the Fast-R2D2 models were trained for 20 epochs using synthetic image pairs generated by applying known transformations (homographies) on random web images [76] and on images of the Aachen Day-Night dataset [91, 93, 123]. We also use additional optical flow matches computed on Aachen Day-Night. For inference, we use the original feature extraction code. Please refer to [79] for more details about the data generation, training, and inference procedures.

A.3. Hyper-parameter selection

In this section, we explain in more details the methodology we followed to find the optimal faster architecture.

In order to find the best set of hyper-parameters for the faster architecture, we grid search the possible variables, which are i) the position of the pooling step: index between 0 and 6 (e.g. a value of 2 means the pooling operation follows the convolution of index 2), ii) the pooling type: AVG or MAX, and iii) the down-sampling factor: 2 or 3.

We observe that any greater down-sampling factor, regardless of the architecture we tried, led to divergence of the training losses. Similarly, more than one pooling step induced large performance drops, so we experimented using only one.

Models nomenclature. We denote the various models with s for the pooling step position, p for the pooling type, and d for the down-sampling factor.

We plot the training losses of the various architectures in Figure 6. Using this, we isolate good candidates for best performing faster architectures, which are 's1_pMAX_d2', 's2_pMAX_d2', 's0_pAVG_d2' and 's1_pAVG_d2'.

We then run localization experiments with these candidate models. In particular, using the same extraction procedure as [81], and the localization pipeline described in the main paper. We evaluate on the Aachen Day Night v1.1 public benchmark. We ran each experiment 4 times and only the best result is kept, to account for small variations in the localization pipeline (due to RANSAC). Table 13 summarizes the results of the chosen candidate architectures.

As can be seen in Table 4 of the main paper, the speed

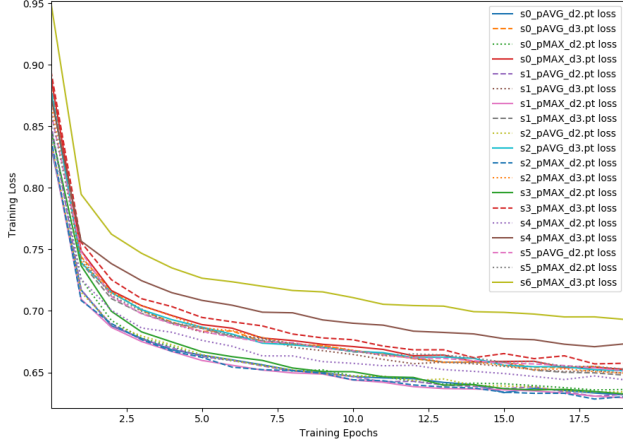


Figure 6. Training losses of the explored down-sampling placements and types.

Model	Avg.	Day			Night		
		all bins	high	mid	low	high	mid
s0_pAVG_d2	90.70	89.4	96.2	99.5	73.3	87.4	98.4
s1_pAVG_d2	90.52	89.4	96.2	99.5	74.3	85.3	98.4
s1_pMAX_d2	90.98	89.9	96.4	99.5	74.3	87.4	98.4
s2_pMAX_d2	90.90	90.2	96.2	99.4	74.3	87.4	97.9

Table 13. Localization performance of candidate architectures on Aachen Day Night v1.1. Final selected architecture in **bold**.

improvement of the chosen architecture is threefold. Interestingly, one would expect the down-sampling step to decrease accuracy in localization, however we observed that it was not the case and this faster architecture is among the best performing methods, as seen in the localization evaluations Tables 4 and 10 of the main paper.

B. Late fusion of global image representations

In the early literature, fusion techniques were often used to combine complementary visual cues measuring the similarity between images [47, 120] or different modalities [32, 28, 125]. Mostly used fusion mechanisms are weighted score averaging (**mean**) or powered product (**power**). Power penalizes severely if one of the scores is low, thus, it can be interpreted as a logical "and". Additionally, the **min** operator explicitly encodes the logical "and" (all scores need to be high) and **max** encodes the logical "or" (a single score needs to be high).

Csurka *et al.* in [28] show that the combination of these operators in general further increases the robustness of the retrieval. Following this idea, together with the mentioned simple operators, we evaluate the following combined fusion operators. **wmp** is a weighted combination of **mean** and **power**:

$$M_{wmp}(q, d) = \beta \cdot \sum_i \rho_i s_i(q, d) + (1 - \beta) \cdot \prod_i s_i(q, d)^{\rho_i}$$

and **wmm** is a weighted combination of **min** and **max**:

$$M_{wmm}(q, d) = (1 - \beta) \max_i(s_i(q, d)) + \beta \min_i(s_i(q, d))$$

where $s_i(q, d)$ is the similarity score between the query q and database image d computed with the representation i . Generalized weighted harmonic mean **gharm** can be obtained using the generalized f-mean operator:

$$M_f(x_1, \dots, x_n) = f^{-1} \left(\sum_{i=1}^n \frac{f(x_i)}{n} \right)$$

with $f(x) = \frac{1}{\gamma+x}$, $x_i = \alpha_i s_i(q, d)$, $\sum_{i=1}^n \alpha_i = 1$, n being the number of different image representations considered.

In addition to score aggregation, rank list aggregation methods are proposed in the literature [7, 47, 120]. To complete our evaluation, we select **round robin** scheduling which creates a combined rank list by selecting new elements from each individual rank list in circular order.

C. Further experimental comparisons

Contrary to the section 4, here we present the results from above with complementary ones, this time organized per dataset.

In detail, if available, in Tables 14 - 23, we present comparisons of:

- the six late fusion operators presented in Section B,
- the four global image representations used in Section 4.3 of the main paper,
- the five local feature types using in Section 4.2,
- state-of-the-art methods (no exhaustive list but the best methods),
- and two sets of COLMAP [95] parameters from Table 2 (config1 and config2).

In addition to the main paper, we also present experimental results on the 12-scenes [110] dataset. We did not include these results in the main paper, because the dataset is already saturated at 100% using the official error thresholds of 5cm and 5°. Instead, in Table 22 we present results using tighter thresholds of 1cm and 1°. Finally, Table 24 presents results of the three variants for image registration (see Section 4.4) using top 1, 5, 10, and 20 retrieved images.

Algorithm	avg. all bins	day			night		
		high	mid	low	high	mid	low
R2D2 40k,GHARM-50,config2	92.45	90.9	96.7	99.5	78.5	91.1	98.0
hloc+SuperGlue [83]	92.15	89.8	96.1	99.4	77.0	90.6	100.0
Fast-R2D2,GHARM-20,config2	91.75	90.3	96.6	99.6	74.9	90.1	99.0
R2D2,GHARM-20,config2	91.68	90.5	96.8	99.4	74.9	90.1	98.4
R2D2,mean and power-20,config2	91.33	90.7	96.8	99.3	73.3	89.5	98.4
Fast-R2D2,APGeM-20,config2	90.98	89.8	96.5	99.5	74.3	87.4	98.4
R2D2,round robin-20,config2	90.70	89.6	96.6	99.4	72.8	87.4	98.4
R2D2,min and max-20,config2	90.70	89.9	96.4	99.2	73.3	88.0	97.4
R2D2,max-20,config2	90.65	89.2	96.0	99.0	73.8	88.0	97.9
R2D2,NetVLAD-20,config2	90.60	88.7	95.1	98.1	74.3	89.5	97.9
R2D2,DELG-20,config2	90.55	90.0	96.0	99.2	73.3	87.4	97.4
R2D2,APGeM-20,config2	90.32	89.9	96.5	99.5	71.2	86.9	97.9
ASLFeat [66],APGeM-20,config2	89.97	87.5	95.4	99.3	73.8	85.9	97.9
RLOCS_v1.0 [37]	89.90	86.0	94.8	98.8	72.3	88.5	99.0
D2-Net,APGeM-20,config2	89.15	85.8	94.3	98.8	70.7	86.9	98.4
R2D2,min-20,config2	88.40	89.1	95.0	98.2	71.2	84.8	92.1
R2D2,DenseVLAD-20,config2	84.93	88.2	94.2	97.3	62.8	79.1	88.0
R2D2,APGeM-20,config1	83.72	60.8	80.9	99.3	75.4	88.0	97.9
COLMAP SIFT,APGeM-20,config2	79.17	87.7	94.2	98.4	51.8	65.4	77.5
COLMAP [95]	66.18	80.2	88.3	93.0	33.0	46.1	56.5

Table 14. Experiments summary for Aachen Day-Night v1.1 [91, 93, 123] (sorted in descending order by average over all bins).

Algorithm	avg. all bins	DUC1			DUC2		
		high	mid	low	high	mid	low
RLOCS_v1.0 [37]	70.10	47.00	71.2	84.8	58.8	77.9	80.9
hloc+SuperGlue [83]	68.57	49.00	68.7	80.8	53.4	77.1	82.4
R2D2,mean and power-50,config2	59.77	39.90	57.6	71.7	48.9	67.2	73.3
Fast-R2D2,GHARM-50,config2	59.55	40.40	63.1	78.3	42.7	64.9	67.9
R2D2,GHARM-50,config2	58.68	39.90	58.1	71.7	45.8	65.6	71.0
DensePV+S (w/ scan-graph) [103]	58.62	40.90	63.6	71.7	42.7	61.8	71.0
R2D2,min and max-50,config2	56.93	37.90	56.6	70.7	44.3	62.6	69.5
R2D2,NetVLAD-50,config2	56.03	36.90	58.1	70.2	38.2	62.6	70.2
R2D2,DenseVLAD-50,config2	56.02	33.80	51.5	67.7	45.0	65.6	72.5
R2D2,min-50,config2	55.85	32.80	54.5	67.7	42.7	65.6	71.8
InLoc [102]	54.80	40.90	58.1	70.2	35.9	54.2	69.5
R2D2,DELG-50,config2	55.17	38.40	56.1	71.7	37.4	59.5	67.9
Fast-R2D2,APGeM-50,config2	54.48	34.80	56.6	73.7	35.9	59.5	66.4
R2D2,max-50,config2	54.20	39.90	55.1	69.2	38.9	58.0	64.1
R2D2,APGeM-50,config2	53.68	38.40	58.6	70.2	37.4	55.7	61.8
R2D2,round robin-50,config2	47.13	33.80	51.5	66.2	29.8	48.1	53.4
R2D2,APGeM-50,config1	41.02	28.30	43.4	60.6	25.2	39.7	48.9
COLMAP [95]	32.13	28.80	43.4	59.6	13.7	20.6	26.7

Table 15. Experiments summary for InLoc [102, 115] (sorted in descending order by average over all bins). R2D2 with 40k keypoints.

Algorithm	avg. all bins	day			night		
		high	mid	low	high	mid	low
Fast-R2D2,APGeM-20,config1 rig seq	80.85	65.9	95.1	100.0	46.2	81.4	96.5
hloc+SuperGlue [83]	80.77	63.8	95.0	100.0	45.0	86.2	94.6
Fast-R2D2,GHARM-20,config1 rig seq	80.17	65.9	95.1	100.0	45.2	80.4	94.4
R2D2,mean and power-20,config1 rig seq	79.93	65.9	95.1	100.0	46.4	79.7	92.5
R2D2,GHARM-20,config1 rig seq	79.20	66.0	95.1	100.0	46.2	76.5	91.4
R2D2,APGeM-20,config1 rig seq	79.17	65.7	95.1	100.0	43.6	76.7	93.9
ASLFeat [66],APGeM-20,config1 rig seq	78.98	64.7	94.9	99.9	45.2	77.4	91.8
R2D2,round robin-20,config1 rig seq	78.78	65.9	95.1	100.0	42.4	75.1	94.2
R2D2,DenseVLAD-20,config1 rig seq	78.17	65.7	95.1	100.0	41.3	74.1	92.8
R2D2,APGeM-20,config1 rig	77.85	65.7	95.1	100.0	43.6	76.0	86.7
R2D2,APGeM-20,config2	77.75	65.9	95.1	99.9	43.4	74.8	87.4
R2D2,min-20,config1 rig seq	77.55	65.8	95.1	100.0	40.8	72.0	91.6
R2D2,min and max-20,config1 rig seq	76.80	65.7	95.1	100.0	41.3	72.5	86.2
R2D2,NetVLAD-20,config1 rig seq	76.28	65.6	95.1	100.0	35.7	70.4	90.9
R2D2,APGeM-20,config1	76.25	65.7	95.1	99.9	41.5	73.0	82.3
R2D2,DELG-20,config1 rig seq	73.50	65.6	94.6	99.6	37.8	64.6	78.8
R2D2,max-20,config1 rig seq	73.30	65.6	94.7	99.7	36.6	63.2	80.0
COLMAP [95] config1 rig seq	50.38	64.2	94.2	99.8	8.9	15.6	19.6
COLMAP [95] config1 rig	49.33	64.2	93.8	98.8	8.4	14.9	15.9
COLMAP [95] config1	47.90	62.9	91.3	94.9	8.4	14.5	15.4

Table 16. Experiments summary for RobotCar Seasons v2 [91] (sorted in descending order by average over all bins).

Algorithm	avg all bins	urban			suburban			park		
		high	mid	low	high	mid	low	high	mid	low
FGSN [57]	98.98	94.1	99.3	100.0	100.0	100.0	100.0	97.6	99.9	99.9
hloc+SuperGlue [83]	98.38	98.1	99.8	99.9	98.3	99.5	100.0	94.2	97.1	98.5
Fast-R2D2,GHARM-20,config1 rig seq	96.87	97.3	99.4	99.8	95.6	97.2	99.4	90.8	94.6	97.7
R2D2,GHARM-20,config1 rig seq	96.38	97.0	99.1	99.8	95.0	97.0	99.4	89.2	93.4	97.5
R2D2,mean and power-20,config1 rig seq	96.36	97.0	99.2	99.7	94.7	97.0	99.5	89.2	93.4	97.5
R2D2,round robin-20,config1 rig seq	96.27	96.9	99.1	99.7	94.8	97.0	99.4	88.8	93.1	97.6
R2D2,min and max-20,config1 rig seq	96.24	96.7	98.9	99.6	95.0	97.1	99.5	88.6	93.2	97.6
R2D2,NetVLAD-20,config1 rig seq	95.94	97.1	99.1	99.8	93.8	96.3	99.1	88.1	92.7	97.5
R2D2,min-20,config1 rig seq	95.77	96.3	98.5	99.4	94.2	96.6	99.2	88.0	92.4	97.3
R2D2,DenseVLAD-20,config1 rig seq	95.66	96.1	98.4	99.4	94.2	96.7	99.1	87.9	92.3	96.8
Fast-R2D2,APGeM-20,config1 rig seq	95.53	97.2	99.3	99.8	95.0	97.0	99.2	85.9	90.8	95.6
R2D2,max-20,config1 rig seq	95.04	96.8	98.9	99.7	94.4	97.0	99.3	84.1	89.2	96.0
DenseVLAD D2-Net [36]	95.02	94.0	97.7	99.1	93.0	95.7	98.3	89.2	93.2	95.0
R2D2,DELG-20,config1 rig seq	95.00	96.6	98.8	99.7	94.1	96.7	99.1	84.7	89.6	95.7
R2D2,APGeM-20,config1 rig seq	94.87	96.7	98.9	99.7	94.4	96.8	99.2	83.6	89.0	95.5
R2D2,APGeM-20,config1 rig	94.30	96.5	98.8	99.5	94.3	96.7	99.1	83.1	87.9	92.8
R2D2,APGeM-20,config2	90.71	95.9	98.1	98.9	89.5	92.1	95.2	78.3	82.0	86.4
R2D2,APGeM-20,config1	89.11	95.8	98.1	98.8	88.9	91.1	93.4	75.5	78.4	82.0
Active Search v1.1 [90]	70.48	81.0	87.3	92.4	62.6	70.9	81.0	45.5	51.6	62.0
COLMAP [95] config1 rig seq	62.73	82.7	87.1	92.1	60.1	68.0	78.8	28.3	30.5	37.0
COLMAP [95] config1 rig	53.98	77.7	80.3	80.8	52.1	56.0	57.5	26.2	27.5	27.7
COLMAP [95] config1	39.50	63.0	65.1	65.3	35.2	37.4	38.3	16.7	17.2	17.3

Table 17. Experiments summary for Extended-CMU [91, 13] (sorted in descending order by average over all bins).

Algorithm	avg. all bins	evening			snow			night		
		high	mid	low	high	mid	low	high	mid	low
hloc+SuperGlue [83]	51.59	35.5	75.0	97.1	0.0	2.4	86.3	31.7	54.4	81.9
R2D2,GHARM-20,config1 rig seq	50.22	32.4	67.4	93.3	0.2	4.1	88.9	30.4	54.2	81.1
R2D2,min and max-20,config1 rig seq	50.00	32.1	67.6	93.4	0.2	3.3	88.7	30.5	54.0	80.2
R2D2,APGeM-20,config1 rig	49.97	31.9	66.6	92.5	0.5	5.8	89.2	30.5	54.2	78.5
R2D2,APGeM-20,config1 rig seq	49.97	31.9	66.6	92.5	0.5	5.8	89.2	30.5	54.2	78.5
R2D2,mean and power-20,config1 rig seq	49.88	31.7	67.0	93.5	0.0	2.7	88.5	30.4	54.4	80.7
Fast-R2D2,APGeM-20,config1 rig seq	49.76	32.3	65.8	91.8	0.3	3.9	89.4	30.2	54.3	79.8
Fast-R2D2,APGeM-20,config1 rig	49.74	32.3	65.8	91.7	0.3	3.9	89.4	30.2	54.3	79.8
R2D2,round robin-20,config1 rig seq	49.61	31.8	66.9	92.0	0.0	3.4	89.6	29.3	54.0	79.5
R2D2,DELG-20,config1 rig seq	49.42	31.3	66.4	92.1	0.2	7.5	85.6	30.2	54.1	77.4
NetVLAD (top50) D2-Net [36]	49.33	29.6	67.8	94.8	6.0	16.4	72.3	25.6	51.6	79.9
Fast-R2D2,GHARM-20,config1 rig seq	49.18	28.9	65.9	92.3	0.2	3.4	89.7	28.6	53.4	80.2
Fast-R2D2,GHARM-20,config1 rig	49.17	28.9	65.9	92.2	0.2	3.4	89.7	28.6	53.4	80.2
R2D2,NetVLAD-20,config1 rig seq	48.99	31.6	66.5	91.0	0.0	2.7	89.6	28.9	52.1	78.5
R2D2,max-20,config1 rig seq	48.89	31.8	65.9	92.4	0.3	2.7	84.6	30.4	54.1	77.8
R2D2,APGeM-20,config2	48.00	33.1	67.8	92.3	0.3	5.3	70.7	30.3	53.5	78.7
Fast-R2D2,APGeM-20,config2	47.49	32.3	66.9	90.9	0.3	5.5	68.8	30.3	53.3	79.1
R2D2,min-20,config1 rig seq	46.47	30.1	63.9	82.5	0.0	1.9	76.2	28.1	54.1	81.4
R2D2,APGeM-20,config1	46.39	31.8	66.3	89.4	0.3	3.9	64.9	30.0	53.4	77.5
Fast-R2D2,GHARM-20,config1	46.08	28.7	65.4	88.8	0.2	3.4	66.6	28.6	53.2	79.8
Fast-R2D2,APGeM-20,config1	45.79	32.2	65.4	88.3	0.2	2.4	61.8	29.8	53.4	78.6
COLMAP [95] rig seq	43.01	32.3	67.9	93.4	0.3	11.3	68.2	18.3	33.8	61.6
COLMAP [95] rig	42.99	32.3	67.9	93.4	0.3	11.3	68.0	18.3	33.8	61.6
R2D2,DenseVLAD-20,config1 rig seq	42.90	27.9	59.7	75.6	0.0	1.9	59.1	29.3	52.9	79.7
COLMAP [95]	40.57	32.1	67.2	92.4	0.3	8.6	56.5	17.3	31.8	58.9

Table 18. Experiments summary for SILDa [14] (sorted in descending order by average over all bins).

Method	%localized (1m, 5.0°)
R2D2,frustum,DenseVLAD-50,config2	85.0
RootSIFT + VVS	84.8
R2D2,frustum,NetVLAD-50,config2	84.1
Direct Matching	83.3
R2D2,frustum,APGeM-50,config2	82.6
R2D2,frustum,DELG-50,config2	82.6
R2D2,distance-20,APGeM-20,config2	79.9
R2D2,APGeM-20,config2	79.1
R2D2,frustum-20,APGeM-20,config2	79.0
COV + RootSIFT	75.4

Table 19. Comparison of variations of our method with top performing state-of-the-art methods on the Baidu-Mall dataset. All baseline results were taken from [101] and, contrary to ours, computed using a Lidar map. *frustum-20* means that only the top 20 images are used, contrary to *frustum*, which uses all overlapping pairs (same for *distance-20* and *APGeM-20*).

Algorithm	Localization Errors			
	avg. all bins	test		
		high	mid	low
Ospace	75.13	57.6	80.6	87.2
MegLoc	72.07	55.9	77.5	82.8
R2D2,GHARM-50,ransaclib	66.23	51.2	71.5	76.0
ASLFeat,OpenIBL-50,config2	61.03	48.0	65.2	69.9
R2D2-APGeM-50,config2	59.77	46.0	64.6	68.7
R2D2-OpenIBL-20,config2	57.70	44.1	62.0	67.0
Onavi	56.50	43.4	61.0	65.1
R2D2-APGeM-20,config2	55.30	42.4	59.7	63.8

Table 20. Experiments summary for Gangnam Station B2 [61] (sorted in descending order by average over all bins).

Method	Median 6D Localization Errors							
	Avg. Median Error	Chess	Fire	Heads	Office	Pumpkin	Stairs	Kitchen
PoseNet [51]	0.23m, 8.1°	0.13m, 4.5°	0.27m, 11.3°	0.17m, 13.0°	0.19m, 5.6°	0.26m, 4.8°	0.35m, 12.4°	0.23m, 5.4°
ActiveSearch [90]	0.04m, 1.2°	0.03m, 0.9°	0.02m, 1.0°	0.01m, 0.8°	0.04m, 1.2°	0.07m, 1.7°	0.04m, 1.0°	0.05m, 1.7°
InLoc [102]	0.04m, 1.4°	0.03m, 1.1°	0.03m, 1.1°	0.02m, 1.2°	0.03m, 1.1°	0.05m, 1.6°	0.09m, 2.5°	0.04m, 1.3°
DSAC++ [19]	0.04m, 1.1°	0.02m, 0.5°	0.02m, 0.9°	0.01m, 0.8°	0.03m, 0.7°	0.04m, 1.1°	0.09m, 2.6°	0.04m, 1.1°
DSAC* [21]	0.02m, 1.3°	0.01m, 1.0°	0.01m, 1.1°	0.01m, 1.9°	0.01m, 1.0°	0.02m, 1.2°	0.03m, 1.2°	0.02m, 1.4°
HACNet [62]	0.03m, 0.9°	0.02m, 0.7°	0.02m, 0.9°	0.01m, 0.9°	0.03m, 0.8°	0.04m, 1.0°	0.03m, 0.8°	0.04m, 1.2°
PixLoc [85]	0.03m, 1.0°	0.02m, 0.8°	0.02m, 0.7°	0.01m, 0.8°	0.03m, 0.8°	0.04m, 1.2°	0.05m, 1.3°	0.03m, 1.2°
hloc + SuperGlue [83]	0.03m, 1.1°	0.02m, 0.9°	0.02m, 0.9°	0.01m, 0.8°	0.03m, 0.9°	0.05m, 1.3°	0.05m, 1.5°	0.04m, 1.4°
Relocalisation Cascade [24]	0.01m, 1.2°	N/A	N/A	N/A	N/A	N/A	N/A	N/A
R2D2,RGBD,APGeM-20,config2	0.03m, 0.9°	0.02m, 0.8°	0.02m, 0.8°	0.01m, 0.7°	0.03m, 0.8°	0.04m, 1.1°	0.04m, 1.1°	0.03m, 1.1°

Table 21. Experiments summary for 7-scenes [99].

Method	12-scenes, Median 6D Localization Errors (mm, °)												
	apt1			apt2			office1			office2			
	avg.	kitchen	living	bed	kitchen	living	luke	gates362	gates381	lounge	manolis	5a	5b
R2D2,APGeM-20,config2	9.3, 0.389	6.8, 0.389	8.2, 0.332	9.5, 0.363	6.9, 0.351	9.5, 0.347	12.0, 0.533	8.7, 0.377	9.6, 0.453	11.5, 0.389	7.4, 0.334	11.1, 0.448	10.3, 0.349
R2D2,RGBD,APGeM-20,config2	9.5, 0.397	6.4, 0.377	8.8, 0.332	8.5, 0.369	7.9, 0.416	8.5, 0.318	11.8, 0.514	8.8, 0.363	10.1, 0.455	13.3, 0.444	7.6, 0.346	9.7, 0.421	12.6, 0.414

Method	12-scenes, percentage of successfully localized images (0.01m, 1.0°)												
	apt1			apt2			office1			office2			
	avg.	kitchen	living	bed	kitchen	living	luke	gates362	gates381	lounge	manolis	5a	5b
R2D2,AP-GeM-20,config2	56.28	73.95	61.26	54.90	76.67	55.01	37.82	58.81	53.09	40.37	71.02	44.27	48.15
R2D2,RGBD,AP-GeM-20,config2	54.33	77.03	57.61	57.35	63.33	61.89	38.94	59.84	48.91	28.13	66.62	53.32	39.01

Table 22. Experiments summary for 12-scenes [110].

Method	Median 6D Localization Errors						
	Avg. Median Error*	Great Court	K. College	Old Hospital	Shop Facade	St M. Church	Street
PoseNet [51]	2.54m, 3.0°	7.00m, 3.7°	0.99m, 1.1°	2.17m, 2.9°	1.05m, 4.0°	1.49m, 3.4°	20.7m, 25.7°
ActiveSearch [90]	0.14m, 0.2°	0.24m, 0.1°	0.13m, 0.2°	0.20m, 0.4°	0.04m, 0.2°	0.08m, 0.3°	N/A
InLoc [102]	0.49m, 0.7°	1.20m, 0.6°	0.46m, 0.8°	0.48m, 1.0°	0.11m, 0.5°	0.18m, 0.6°	N/A
DSAC++ [19]	0.19m, 0.3°	0.40m, 0.2°	0.18m, 0.3°	0.20m, 0.3°	0.06m, 0.3°	0.13m, 0.4°	-
DSAC* [21]	0.21m, 0.3°	0.49m, 0.3°	0.15m, 0.3°	0.21m, 0.4°	0.05m, 0.3°	0.13m, 0.4°	-
HACNet [62]	0.16m, 0.3°	0.28m, 0.2°	0.18m, 0.3°	0.19m, 0.3°	0.06m, 0.3°	0.09m, 0.3°	N/A
PixLoc [85]	0.15m, 0.2°	0.30m, 0.1°	0.14m, 0.2°	0.16m, 0.3°	0.05m, 0.2°	0.10m, 0.3°	N/A
hloc + SuperGlue [83]	0.11m, 0.2°	0.16m, 0.1°	0.12m, 0.2°	0.15m, 0.3°	0.04m, 0.2°	0.07m, 0.2°	N/A
R2D2,APGeM-20,config2	0.06m, 0.1°	0.10m, 0.0°	0.05m, 0.1°	0.09m, 0.2°	0.02m, 0.1°	0.03m, 0.1°	0.10m, 0.3°

Table 23. Experiments summary for Cambridge Landmarks [52]. Note that the average median error is computed excluding the Street scene since only 2 methods (including ours) report results for this.

Datasets	Algorithm	percentage of successfully localized images							
Aachen Day-Night v1.1	local features,map pairs,query pairs,method	avg. all bins	day			night			Accuracy thresholds Aachen high: 0.25m, 2° mid: 0.5m, 5° low: 5m, 10°
	R2D2,frustum,APGeM-20,COLMAP config2	90.63	high	mid	low	high	mid	low	
	R2D2,frustum,APGeM-20,pycolmap	90.63	89.9	96.4	99.4	73.8	86.4	97.9	
	R2D2,frustum,APGeM-20,ransaclib	90.62	90.1	96.5	99.5	73.3	85.9	98.4	
	R2D2,frustum,APGeM-10,COLMAP config2	89.27	88.8	96.1	99.4	69.1	85.9	96.3	
	R2D2,frustum,APGeM-10,pycolmap	89.52	87.3	95.3	99.5	71.2	86.9	96.9	
	R2D2,frustum,APGeM-10,ransaclib	89.67	88.4	96.2	99.5	71.2	85.3	97.4	
	R2D2,frustum,APGeM-5,COLMAP config2	88.17	87.4	95.4	99.0	65.5	84.8	96.9	
	R2D2,frustum,APGeM-5,pycolmap	88.12	87.3	95.4	98.9	65.5	85.3	96.3	
	R2D2,frustum,APGeM-5,ransaclib	88.08	86.2	94.3	99.2	65.5	85.9	97.4	
	R2D2,frustum,APGeM-1,COLMAP config2	84.67	81.8	92.1	97.2	62.3	75.4	99.2	
	R2D2,frustum,APGeM-1,pycolmap	82.92	81.9	91.4	97.0	60.2	75.9	91.1	
	R2D2,frustum,APGeM-1,ransaclib	83.30	81.9	90.8	97.2	60.7	77.0	92.2	
Gangnam Station B2	local features,map pairs,query pairs,method	avg. all bins	test			validation			Accuracy thresholds Gangnam B2 high: 0.1m, 1° mid: 0.25m, 2° low: 1m, 5°
	R2D2,distance-50,APGeM-20,COLMAP config2	53.35	high	mid	low	high	mid	low	
	R2D2,distance-50,APGeM-20,pycolmap	55.97	44.3	62.5	66.9	38.1	59.6	64.4	
	R2D2,distance-50,APGeM-20,ransaclib	56.12	44.5	62.4	67.0	38.7	59.9	64.2	
	R2D2,distance-50,APGeM-10,COLMAP config2	51.45	39.9	57.3	61.8	34.6	55.5	59.6	
	R2D2,distance-50,APGeM-10,pycolmap	52.67	41.0	58.1	62.5	35.7	56.7	62.0	
	R2D2,distance-50,APGeM-10,ransaclib	52.92	41.0	58.3	62.5	36.2	57.6	61.9	
	R2D2,distance-50,APGeM-5,COLMAP config2	46.98	37.0	53.0	57.0	31.1	49.5	54.3	
	R2D2,distance-50,APGeM-5,pycolmap	47.63	37.4	53.1	57.4	31.9	50.2	55.8	
	R2D2,distance-50,APGeM-5,ransaclib	47.75	37.4	53.6	57.7	32.0	50.3	55.5	
	R2D2,distance-50,APGeM-1,COLMAP config2	34.35	27.0	39.0	43.2	21.9	35.5	39.5	
	R2D2,distance-50,APGeM-1,pycolmap	34.42	27.4	38.9	42.8	22.4	35.5	39.5	
	R2D2,distance-50,APGeM-1,ransaclib	34.88	27.4	39.6	43.2	22.5	36.5	40.1	
Baidu-mall	local features,map pairs,query pairs,method	avg. all bins	all			Accuracy thresholds Baidu-mall high: 0.25m, 2° mid: 0.5m, 5° low: 5m, 10°			
	R2D2,frustum,APGeM-20,COLMAP config2	71.77	high	mid	low				
	R2D2,frustum,APGeM-20,pycolmap	72.97	60.0	75.0	83.9				
	R2D2,frustum,APGeM-20,ransaclib	73.13	59.9	75.6	83.9				
	R2D2,frustum,APGeM-10,COLMAP config2	69.30	56.3	71.4	80.2				
	R2D2,frustum,APGeM-10,pycolmap	70.03	57.6	71.9	80.6				
	R2D2,frustum,APGeM-10,ransaclib	70.17	57.7	72.2	80.6				
	R2D2,frustum,APGeM-5,COLMAP config2	66.83	55.1	68.4	77.0				
	R2D2,frustum,APGeM-5,pycolmap	67.07	55.3	68.5	77.4				
	R2D2,frustum,APGeM-5,ransaclib	67.57	56.0	69.4	77.3				
	R2D2,frustum,APGeM-1,COLMAP config2	55.83	45.2	57.2	65.1				
	R2D2,frustum,APGeM-1,pycolmap	55.97	45.3	57.6	65.0				
	R2D2,frustum,APGeM-1,ransaclib	56.17	45.6	57.8	65.1				

Table 24. Comparison of different variants of our pipeline. We use R2D2 and APGeM with top 1, 5, 10, and 20 for all variants. The maps are created using pairs selected by frustum overlap.